

A simple model for regolith formation by chemical weathering

Jean Braun, Jonathan Mercier, François Guillocheau, Cécile Robin

▶ **To cite this version:**

Jean Braun, Jonathan Mercier, François Guillocheau, Cécile Robin. A simple model for regolith formation by chemical weathering. Journal of Geophysical Research: Earth Surface, 2016, 121 (11), pp.2140-2171 10.1002/2016JF003914 . insu-01384700

HAL Id: insu-01384700
https://insu.hal.science/insu-01384700

Submitted on 15 Nov 2016

HAL is a multi-disciplinary open access archive for the deposit and dissemination of scientific research documents, whether they are published or not. The documents may come from teaching and research institutions in France or abroad, or from public or private research centers.

L'archive ouverte pluridisciplinaire **HAL**, est destinée au dépôt et à la diffusion de documents scientifiques de niveau recherche, publiés ou non, émanant des établissements d'enseignement et de recherche français ou étrangers, des laboratoires publics ou privés.

AGU PUBLICATIONS

JGR

Journal of Geophysical Research: Earth Surface

RESEARCH ARTICLE
10.1002/2016JF003914

A simple model for regolith formation by chemical weathering

Jean Braun[1,2], Jonathan Mercier[1], Francois Guillocheau[3], and Cécile Robin[3]

[1]ISTerre, Université Grenoble Alpes and CNRS, Grenoble, France, [2]Now at Helmholtz Centre Potsdam, German Research Center for Geosciences (GFZ), Telegrafenberg, Potsdam, Germany, [3]Géosciences Rennes, Université Rennes 1 and CNRS, Rennes, France

Key Points:
- New model for regolith formation by chemical weathering predicts regolith geometry and thickness in a range of environments
- Surface slope, precipitation, and exhumation rate are most important controlling parameters
- We defined two dimensionless numbers that control the thickness and geometry of the regolith

Correspondence to:
J. Braun,
jean.braun@univ-grenoble-alpes.fr

Citation:
Braun, J., J. Mercier, F. Guillocheau, and C. Robin (2016), A simple model for regolith formation by chemical weathering, *J. Geophys. Res. Earth Surf.*, *121*, doi:10.1002/2016JF003914.

Received 7 APR 2016
Accepted 12 OCT 2016
Accepted article online 18 OCT 2016

Abstract We present here a new model for the formation of regolith on geological timescales by chemical weathering based on the assumption that the rate of chemical weathering is primarily controlled by the ability of groundwater to transport solute away from the reacting solid-fluid interface and keep the system from reaching equilibrium (saturation). This allows us to specify the rate of propagation of the weathering front as linearly proportional to the pore fluid velocity which we obtain by computing the water table geometry in the regolith layer. The surface of the regolith layer is affected by mass transport and erosion. The main prediction of the model is that the geometry of the regolith, i.e., whether it is thickest beneath topographic highs or topographic lows, is controlled by the value of a dimensionless number, which depends on the square of the surface slope, the hydraulic conductivity, and local precipitation rate, but is independent of the chemical weathering rate. In orogenic environments, where regolith formation by chemical weathering competes with surface erosion, the model predicts that the existence and thickness of the regolith layer are controlled by the value of another dimensionless number which is the ratio between the timescale for erosion and the timescale for weathering. The model also predicts that in anorogenic areas, regolith thickness increases as the square root of time, whereas in orogenic environments, a steady state regolith thickness can be achieved, when the propagation of the weathering front is equal to erosion rate.

1. Introduction

Chemical weathering of continental interiors is one of the essential processes by which the Earth's surface evolves in response to surface uplift generated by tectonics and mantle flow and therefore by which crustal thickness and composition evolve on geological timescales [*Lee et al.*, 2008]. In tectonically active areas, chemical weathering is often regarded as a "softening agent" that renders surface rocks more prone to physical erosion by river bedrock incision and landsliding or other hillslope processes [*Ahnert*, 1977]. In these environments, the formation of a regolith layer, the product of weathering, is therefore often regarded as resulting from a dynamical equilibrium between the propagation of a weathering front at depth and the removal or transport of soil at the surface by erosion (see *Phillips* [2005] for a complete discussion on the links between landscape evolution and weathering at a range of spatial and temporal scales). Consequently, the regolith layer tends to be relatively thin, i.e., a few meters at the most, and strongly controlled by surface topography and slope. Away from tectonic areas, chemical weathering often dominates over physical erosion, and much thicker regolith layers can develop [*Berry and Ruxton*, 1959; *Thomas*, 1966], reaching thickness of several hundred meters under extreme conditions of tectonic stability, high precipitations, and warm temperature [*Vasconcelos et al.*, 1994; *Carmo and Vasconcelos*, 2004].

Understanding the process and rate of chemical weathering, and its relative contribution to surface evolution in comparison to physical erosion, is also of key importance to quantify the carbon flux from the solid Earth to the hydrosphere and its control on atmospheric carbon dioxide concentration and global climate [*Dupré et al.*, 2003]. There is still much debate on how much weathering contributes to the long-term evolution of our planet's climate, for example, its effect on Cenozoic global cooling and its acceleration in the Quaternary [*Francois and Goddéris*, 1998].

With rock fracturing, chemical weathering is also the main process by which impermeable bedrock is transformed into an aquifer [*Lachassagne et al.*, 2011]. Understanding and quantifying the processes by which this transformation takes place is also of prime importance if we wish to characterize and map water flow at or near

©2016. American Geophysical Union. All Rights Reserved.

the Earth's surface [*Gleeson et al.*, 2015; *Pelletier et al.*, 2016]. The thickness and characteristics of the regolith layer are key controls on catchment hydrology via infiltration of precipitation, resurgence, and evapotranspiration through vegetation cover and vegetation type. There is even recent evidence that groundwater flow may affect the thermal structure of the continental lithosphere [*Kooi*, 2016].

Remarkably, relatively few quantitative models exist that can predict the rate of formation and thus the thickness of the regolith in both orogenic and anorogenic environments (see next section for a short overview) and that could be incorporated in models of landform evolution, for example. In this paper, we present a new model for the formation and evolution of the regolith that assumes that chemical alteration is the primary mechanism controlling the propagation of the weathering front and that it is the ability of the flowing water to keep the system away from saturation that controls the rate of dissolution. The model is relatively simple because our objective is to incorporate it in a model of long-term landscape evolution; yet it predicts a range of behaviors, depending on local surface slope, precipitation rate, and tectonic uplift rate that are testable against observations.

2. General Concepts and Existing Models

Chemical weathering rates are primarily controlled by the presence and flow of water [*Lasaga et al.*, 1994]. There is now broad consensus that mineral dissolution is controlled not only by the kinetics of the chemical reactions at play during dissolution [*Berner*, 1978] but also by the concentration of dissolved minerals in the fluid phase [*Lasaga et al.*, 1994; *Maher*, 2011]. Where the residence time of water is low (high fluid velocity), kinetics controls the rate of weathering, whereas in situations where fluid residence time is high (low fluid velocity), the rate of weathering is mostly controlled by the ability of the system to remove the product of the weathering from the rock-water interface. This can, in turn, be achieved by either diffusion or advection of the solute [*Lichtner*, 1988], the competition between the two processes being measured by the value of the dimensionless Peclet number

$$Pe = \frac{vL}{\kappa} \tag{1}$$

where v is the fluid velocity, L the thickness of the weathering layer, and κ the diffusivity of the solute in the fluid. For typical values of $\kappa \approx 10^{-8}$ m^2/s, $v \geq 1$ m/yr$= 3.15\times10^{-7}$ m/s, and $L \geq 1$ m, Pe is much greater than unity and advection dominates. This leads to the important consequence that it is the residence time of water in the weathering bedrock [*Maher*, 2010, 2011; *Maher and Druhan*, 2014] and thus the velocity of the water that is likely to be the primary control on the rate of weathering. Some have argued, however, that, in some systems, diffusion may be the dominant process for solute transport, because of the very low porosity, permeability, and thus flow rate at the regolith-bedrock interface [*Lebedeva et al.*, 2007].

Models of varying complexity have been developed to explain the formation and evolution of regolith profiles in a variety of environments. One of the simplest and most widely used is based on the assumption that the availability of water at the regolith-bedrock interface is controlled by the thickness of the regolith layer and leads to an inverse exponential dependence between regolith/soil depth, B, and the rate of regolith formation, $\partial B/\partial t$ [*Ahnert*, 1977]

$$\frac{\partial B}{\partial t} = \dot{W}_0 \, \mathrm{e}^{-B/B_0} \tag{2}$$

where $\dot{W}_0$ is the bare rock rate of regolith formation and B_0 a length scale that can be regarded as the mean regolith thickness that will be achieved by this process alone, typically a few meters at most. Such a relationship has been evidenced in several environments [*Heimsath et al.*, 1997, 2012], especially when applied to soil thickness, where soil is the upper part of the regolith that is actively transported by surface processes. This relationship has also served as the basis of many conceptual and numerical models of regolith and/or soil formation and, coupled with a model of surface transport and erosion, has been used to explain the dynamics of regolith-mantled hillslopes and, more generally, the distribution of regolith thickness in mountain belts [*Braun et al.*, 2001; *Ferrier and Kirchner*, 2008; *Yoo et al.*, 2009; *Gabet and Mudd*, 2009; *Vanwalleghem et al.*, 2013; *Carretier et al.*, 2014]. A slightly more evolved or so-called "humped" relationship has been introduced by *Carson and Kirkby* [1972] to account for the fact that under thin soil/regolith or exposed bedrock conditions, surface runoff dominates and chemical weathering is reduced, an observation already made by *Gilbert* [1877] in the Henry Mountains. There might also be a minimum soil thickness required for animals and plants to

develop [*Wilkinson*, 2015], and vegetation has a potentially strong control on chemical weathering rates through the role of carboxylic acids on albite dissolution [*Franklin et al.*, 1994]. This humped model predicts an optimal soil or regolith thickness where a maximum in weathering rate is achieved. A similar behavior can be obtained by assuming a characteristic timescale for reaction kinetics [*Hilley et al.*, 2010]. These simple models have been widely used to predict soil or regolith thickness, especially in tectonic environments, and the rapid evolution toward a balance between production (transformation of bedrock into regolith) and surface transport [*Yoo et al.*, 2009; *Gabet and Mudd*, 2009; *Hilley et al.*, 2010; *Vanwalleghem et al.*, 2013; *Carretier et al.*, 2014].

At the other end of the spectrum, very complex models have been designed to study the time evolution of a reactive porous medium by solution/dissolution of mineral phases, as well as the precipitation of secondary minerals and their effect on porosity and permeability [e.g., *Mayer et al.*, 2002; *Moore et al.*, 2012]. These models are useful to predict groundwater and river geochemistry, but, due to their complexity, they require a detailed knowledge of local model parameters and, therefore, are not easily scalable to geological timescales.

Intermediate complexity models have also been developed that combine chemical models, sometimes involving several reacting minerals, with advection-diffusion transport models of the solute [*Lebedeva et al.*, 2007, 2010; *Lebedeva and Brantley*, 2013]. These are, however, based on a highly simplified hydrological model, commonly assuming a constant and uniform Darcy flow velocity within the regolith layer, potentially missing an important feedback between regolith thickness and weathering front propagation. They explain, however, the broad classification of regolith formation regimes [*Riebe et al.*, 2001, 2004; *West et al.*, 2005]: a weathering-limited regime and thus climate-controlled regime in tectonically active areas versus a transport- or erosion-limited regime in tectonically quiescent areas [*Lebedeva et al.*, 2007; *Li et al.*, 2014]. They also predict that, in rapidly uplifting and eroding regions, a local equilibrium can be achieved between surface erosion/uplift and weathering [*Lebedeva et al.*, 2010], whereas in noneroding areas and under the assumption that solute transport is dominated by diffusion, regolith thickness should increase as the square root of time [*Lebedeva et al.*, 2010]. More recently, *Rempe and Dietrich* [2014b] computed steady state regolith geometry on a hillslope undergoing uplift and surface erosion based on a simple groundwater flow model in the underlying bedrock. Assuming that the water table corresponds to the weathering front, they arrive at the conclusion that regolith thickness is controlled by the ratio of the slope of the water table to the surface slope.

Much emphasis has, however, been put on modeling and understanding chemical weathering and the formation of the regolith in tectonically active areas, in parts, to quantify the relative contribution of chemical versus physical erosion in these environments and the potential feedback between orogeny (which brings fresh bedrock to the surface) and climate, through CO_2 consumption by weathering and subsequent reduction in greenhouse effect [*Gaillardet et al.*, 1999]. Relatively little work has, however, been devoted to the formation of thick regolith profiles in tectonically quiescent areas although, due to their larger extent, they may in fact dominate the contribution to atmospheric CO_2 concentration from weathering on geological timescales [*Goddéris and Francois*, 1995]. Simple models based on an exponential or humped relationship between regolith thickness and weathering rate cannot explain the formation of thick regolith profiles as commonly observed in continental interiors where regolith thicknesses are in excess of several tens of meters [*Berry and Ruxton*, 1959; *Thomas*, 1966; *Vasconcelos et al.*, 1994; *Carmo and Vasconcelos*, 2004]. The most plausible explanation for the formation of these thick profiles is that the water is not simply percolating vertically through the overlying regolith but is traveling laterally, potentially in response to regional-scale topographic gradient. This requires the development of a fully coupled two-dimensional model that combines groundwater flow and regolith formation.

This is what we propose to do here. We first describe the three main components of the model (hydrological model, weathering front propagation model, and surface erosion/transport model) and how they relate to each other. To study the model behavior, we first describe results obtained under the simplest geometrical conditions (a hill of constant and uniform slope that is not affected by tectonic uplift or surface erosion). We introduce a dimensionless number that is used to define two regimes predicting different regolith geometries. The model is then used to study the evolution of the regolith system in a tectonically active environment, i.e., by imposing a uniform surface uplift and introducing erosional processes at the surface. By introducing a second dimensionless number, we define the conditions necessary for the existence of a steady state solution for regolith formation in an actively uplifting and eroding landscape. We then show how the conclusions regarding regolith geometry in anorogenic settings can be extrapolated to active tectonic environments. A few case

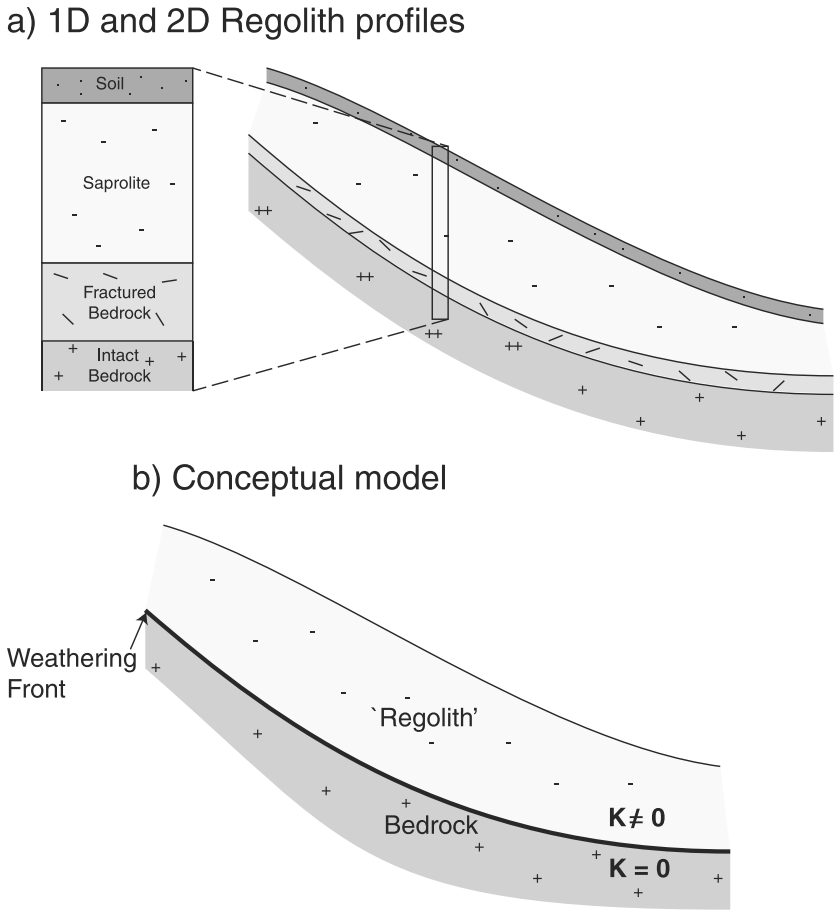


Figure 1. (a) Schematic representation of a regolith on top of a sloping hill comprising a mobile soil layer, a saprolite layer (or in-place weathered rock), and a fractured bedrock layer. (b) Our idealized representation of it where the fractured bedrock layer has been made into a weathering front.

examples are used to illustrate how the value of the two controlling dimensionless numbers can be extracted from the geometry of the regolith and can, in turn, be used to quantify important timescales concerning the weathering process. We conclude by reviewing the consequences of our model for the distribution of regolith at the Earth's surface as a function of tectonic uplift, surface erosion, and precipitation rate and by highlighting future applications and developments of the model, including the need to implement it in a 2-D model of landscape evolution.

3. The Model

A regolith profile (Figure 1a) is commonly described as made of a (i) superficial soil layer, which represents the actively transported upper part of the regolith; (ii) a saprolite layer made of relatively undeformed but strongly weathered rocks; and (iii) a layer of fractured (permeable) bedrock overlying the "intact" or impermeable bedrock. The evolution of this system is controlled by surface transport and the rate of transformation of bedrock into regolith by weathering.

3.1. Component 1: Subsurface Hydrology

Our simplified hydrological model (Figure 1b) comprises a permeable "regolith" layer that includes the soil and saprolite layers and is assumed to be characterized by one *effective hydraulic conductivity*, K, separated from the underlying impermeable bedrock by the weathering front. This simplified, bimodal view of the hydraulic system between a porous regolith and an impermeable bedrock stems from the observation that as weathering intensity increases, so does hydraulic conductivity [*White et al.*, 2001; *Brantley and White*, 2009]. Conceptually, the fractured bedrock layer becomes the weathering front, i.e., where the primary weathering

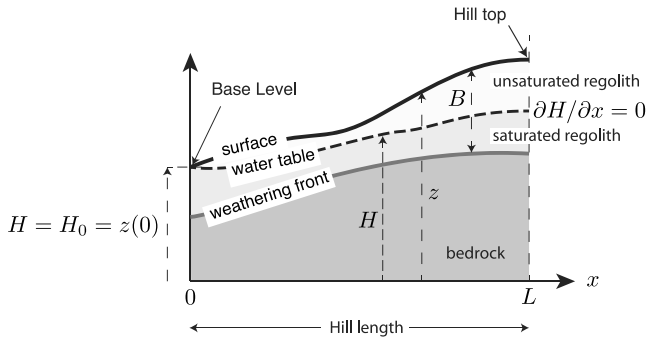


Figure 2. Geometry of the hydrological problem solved in our model and boundary conditions. We consider a topographic feature (a "hill") of length L and height $z(x)$ for $0 < x < L$ that has evolved to form a regolith layer of thickness $B(x)$ by downward propagation of a weathering front. Height of the weathering front is $z - B$. The regolith is traversed by the water table of height $H(x)$. Above the water table the regolith is unsaturated; below it is saturated.

processes are most active. This conceptual model reflects, in part, the common observation that the layer of fractured bedrock is thin in comparison to the total regolith thickness and/or that the transition between altered and intact bedrock at the base of many weathering profiles is sharp, which has led to the concept of a weathering front [*Thomas*, 1966]. This concept is also supported by widespread observations of a sharp gradient in weathering intensity at the base of the weathering profile, as measured by the chemical depletion fraction of immobile elements, for example, [*Riebe et al.*, 2004].

The flow of water within an unconfined aquifer in a homogeneous, permeable layer of thickness $B(x)$ (in meter) beneath a topographic surface $z(x)$ (in meter) (see Figure 2) obeys the following differential equation:

$$\frac{\partial}{\partial x} K(H(x) - z(x) + B(x)) \frac{\partial H(x)}{\partial x} + P(x) = 0 \tag{3}$$

assuming steady state and following the Dupuit-Forchheimer assumptions that flow is dominantly lateral and that discharge is proportional to the saturated aquifer thickness, $H - z + B$. $H(x)$ is the height of the surface of the water table (in meter), K is hydraulic conductivity (in m/yr), and $P(x)$ is *precipitation rate* (in m/yr) or more exactly the *infiltration rate* (precipitation minus evapotranspiration and surface runoff). In the remainder of this paper, we will refer to $P(x)$ as the precipitation rate to indicate that the primary control on $P(x)$ is climate. Here we assume that the aquifer is fully contained within the regolith layer and that the complex, probably spatially and time-varying hydraulic conductivity of the regolith layer, can be represented by a constant or effective conductivity. This is justified by observations and model results that single precipitation or snowmelt events at the surface are felt deeply in the regolith layer [see, e.g., *Salve et al.*, 2012; *Langston et al.*, 2011] showing that the top and bottom of the regolith are hydraulically strongly connected. It has also been recently shown [*Maher and Druhan*, 2014] that it is the mean transit time of water that controls the rate of weathering and that small-scale heterogeneities in hydraulic properties play a second-order role only.

In the remainder of this paper, we compute the solution of this equation beneath a hill (or topographic feature) of length L by imposing the following boundary conditions:

$$H|_{(x=0)} = H_0 = z|_{x=0} = z_b \quad \text{and} \quad \left.\frac{\partial H}{\partial x}\right|_{(x=L)} = 0 \tag{4}$$

This corresponds to assuming that there is a stream (or a large body of water) at the base of the hill and that the right-hand side of the model is a topographic/drainage divide.

For the specific geometry considered here (Figure 2), equation (3) can be simplified by integrating it from $x' = L$ to x to give

$$\int_L^x \left[\frac{\partial}{\partial x'} K(H - z + B) \frac{\partial H}{\partial x'}\right] \mathrm{d}x' + \int_L^x P \, \mathrm{d}x' = 0 \tag{5}$$

and

$$K(H - z + B) \frac{\partial H}{\partial x} + \int_L^x P \, \mathrm{d}x' = 0 \tag{6}$$

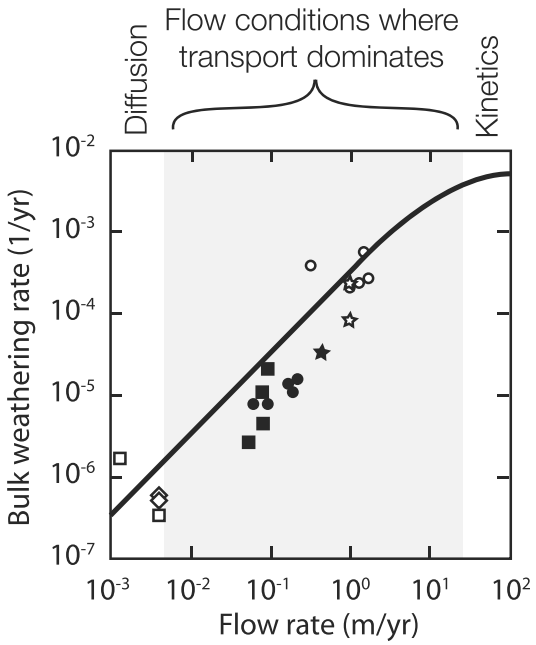


Figure 3. Relationship between weathering rate and flow rate derived from field observations (reproduced from *Maher* [2010]). See original paper for exact references to data.

using $\frac{\partial H}{\partial x}|_{(x=L)} = 0$. It is interesting to note here that, in this formulation, the length of the system, where a "no flow" boundary condition ($\partial H/\partial x = 0$) has been imposed, only appears as the upper bound of a definite integral of net precipitation rate. This implies that at $x = L$, where the integral of net precipitation is nil, two possibilities exist: either $\partial H/\partial x = 0$ (no flow condition) or $H - z + B = 0$ (the water table is in contact with the bedrock). Here we make the implicit assumption that the water table has to be located within the regolith, because the bedrock is assumed to be impermeable.

We have developed an efficient way to solve this equation numerically (Appendix A) and have tested it against a simple analytical solution (Appendix B).

3.2. Component 2: Weathering Front Propagation

In nature, the propagation of the weathering front (fractured bedrock layer) is probably controlled by both the chemical weathering rate (transformation of bedrock into regolith) and the process that is responsible for the fracturing of bedrock. Here we assume that the rate of propagation of the weathering front is primarily controlled by the chemical weathering rate and not the fracturing process. This assumption is mostly driven by the recognition that the vertical propagation of fracturing is, at present, poorly constrained and/or understood.

Further assuming that weathering is transport limited, i.e., that it is controlled by the ability of the system to remove the weathering products by aqueous transport, one can show that the bulk rate of weathering, R_d, is an exponential function of flow rate or fluid velocity, v [*Maher*, 2010]

$$R_d = 10^{-2.3}\left[1 - e^{-0.06\pm0.008v}\right] \tag{7}$$

where R_d is expressed in yr^{-1} and v in m/yr. This relationship is supported by experimental data as shown in Figure 3 [from *Maher*, 2010]. At fast flow rates, the kinetics of the chemical reactions at play during dissolution may become important [*Berner*, 1978], whereas at low flow rates, transport of the solute in the aqueous form may be dominated by diffusion [*Lichtner*, 1988]. For a wide range of flow values, however, this relationship between weathering rate and flow rate is quasi-linear (Figure 3) and simple mass balance considerations lead to a relationship between the rate of propagation of the weathering front, $\frac{\partial B}{\partial t}$, and the fluid flow rate (or velocity) in the weathering front, v [*Ortoleva et al.*, 1987; *Lichtner*, 1988; *Brantley and White*, 2009; *Maher*, 2010]

$$\frac{\partial B}{\partial t} = v\frac{C_{eq}V_m}{M_p} \tag{8}$$

where C_{eq} is the solubility of the weathered mineral (in mol/L), V_m its molar volume (in L/mol), and M_p its volume fraction in the protolith.

The fluid velocity in the regolith layer, v_r, is controlled by the slope of the surface of the water table

$$v_r = K\frac{\partial H}{\partial x} \tag{9}$$

We have assumed that the bulk of the transformation from bedrock to regolith takes place in a thin layer of fractured bedrock which we equated to the weathering front. Assuming that the fractured rock layer (which we assume, here, is the weathering front) is thinner than the regolith layer, water flow is mostly confined to the

regolith layer and the gradient of the surface of the water table (and thus water velocity) is mostly controlled by the hydraulic conductivity of the regolith. The velocity of fluid in the fractured rock layer and thus in the weathering front can be approximated by (Appendix C)

$$v = \frac{K_f}{K} v_r \tag{10}$$

where K_f is the permeability of the fractured bedrock (weathering front).

We can finally write that the rate of propagation of the regolith-bedrock interface, B, is proportional to the gradient of the water table

$$\frac{\partial B}{\partial t} = FK \frac{\partial H}{\partial x} \tag{11}$$

where F is a dimensionless parameter that we name the *weathering rate constant* and assume to be mostly determined by rock type and given by

$$F = \frac{K_f}{K} \frac{C_{\text{eq}} V_m}{M_p} \tag{12}$$

Considering that in granitic rocks plagioclase is the weathering rate controlling mineral, for which $C_{\text{eq}} = 350 \times 10^{-6}$ mol/L, $V_m \approx 10^{-1}$ L/mol [*Lasaga et al.*, 1994], and $M_p \approx 0.15$ [*Anderson and Dietrich*, 2002], we can estimate a range of possible values for F to be

$$F = \left[10^{-1} - 10^{-2}\right] \frac{350 \times 10^{-6} \times 10^{-1}}{0.15} \approx \left[10^{-5} - 10^{-6}\right] \tag{13}$$

assuming that the hydraulic conductivity of fractured bedrock is 1 to 2 orders of magnitude lower than that of the overlying regolith [*Bear*, 1979]. For silicate glass in basalt, $C_{\text{eq}} \times V_m = 10^{-4}$ [*Alexander et al.*, 1954] and a typical basalt contains 30% glass, which gives

$$F_{\text{Basalt}} \approx 3 \times F_{\text{Granite}} \tag{14}$$

Finally, we note that this simple model could be improved to include a limit on weathering rate at high flow velocities (the upper right section of the curve shown in Figure 3):

$$\frac{\partial B}{\partial t} = v_0 F \left(1 - \mathrm{e}^{-v_r / v_0}\right) \tag{15}$$

where v_0 is the fluid velocity over which dissolution is controlled by reaction kinetics. A temperature dependence on weathering rate could also be introduced in our model by making use of the well-known temperature dependence of mineral solubility which can be expressed as a simple Arrhenius relationship [*Rimstidt*, 1997]

$$C_{\text{eq}} = C_{\text{eq},0}\, \mathrm{e}^{-Q/RT} \tag{16}$$

where T is temperature (in K) and Q an activation energy (in J/mol).

3.3. Component 3: Surface Erosion and Tectonic Uplift

We now wish to investigate the effects of tectonic uplift and surface erosion/transport on the thickness of the regolith layer and, consequently, on the geometry of the water table and on the propagation of the weathering front. To do this, we will assume that it is the ability of surface processes to transport the regolith which sets the pace at which material is eroded and transported at/near the surface. We further assume that the surface transport/flux of sediment, q (expressed in m^2/yr), is simply proportional to the surface slope, S (in m/m)

$$q_s = -K_D S \tag{17}$$

where K_D is a *linear transport coefficient* (in m^2/yr). This simple representation of surface processes can be easily improved to take into account that only the soil layer of thickness D (in meter) is transported. Soil thickness

can be computed by assuming a simple exponential relationship between soil thickness and soil production rate [*Heimsath et al.*, 1997]

$$\frac{\partial D}{\partial t} = \dot{D}_0 \, e^{-D/D_0} \tag{18}$$

and that soil thickness is limited by regolith thickness, i.e., $D(x) < B(x)$. $\dot{D}_0$ is the soil production rate at zero soil depth (in m/yr), and D_0 is the thickness of soil (in meter) necessary to reduce the production rate by a factor e. Assuming that the soil behaves like a thin viscous sheet at the surface of the landscape leads to a nonlinear dependence of soil transport on soil thickness and surface slope [*Selby*, 1993; *Braun et al.*, 2001]

$$q_s = -K_V D^m S^n \tag{19}$$

with $m \in [1.2 - 1.67]$ and $n \in [0.5 - 0.7]$ [*Herman and Braun*, 2006].

For the sake of simplicity, we will mostly use, however, the linear relationship between soil flux and slope (i.e., equation (17)) and show that it does not have major implications for the results we present here. Assuming conservation of mass, the rate of evolution of surface topography, z, with time is given by

$$\frac{\partial z}{\partial t} = -\frac{\partial q_s}{\partial x} = \frac{\partial}{\partial x} K_D \frac{\partial z}{\partial x} = K_D \frac{\partial^2 z}{\partial x^2} \tag{20}$$

which takes the form of a diffusion equation, if K_D the soil transport coefficient or diffusivity is assumed constant and uniform. Note that the value of the transport coefficient is poorly determined, especially when, like here, it is meant to represent a broad range of hillslope processes, from soil creep to landsliding [*Martin and Church*, 1997], and may range from 10^{-2} to 10^2 m^2/yr [*Martin*, 2000].

This equation can be completed by adding a tectonic uplift term, U_0 (in m/yr), which we will assume constant over the length L. The surface evolution equation becomes

$$\frac{\partial z}{\partial t} = K_D \frac{\partial^2 z}{\partial x^2} + U_0 \tag{21}$$

and the weathering front propagation equation becomes

$$\frac{\partial B}{\partial t} = FK \frac{\partial H}{\partial x} + \frac{\partial z}{\partial t} - U_0 = FK \frac{\partial H}{\partial x} + K_D \frac{\partial^2 z}{\partial x^2} \tag{22}$$

4. Model Predictions in Anorogenic Areas

We first investigate the model behavior under the assumptions of constant surface slope and zero uplift velocity, characteristics of what we will term "anorogenic" settings or areas. Combining the hydraulic equation (6) with the weathering front equation (11), we introduce an interesting series of potential couplings that may lead to feedbacks between regolith thickness (B) and water table surface height (H). This is because flow in the aquifer is controlled by the water table surface gradient, which is controlled by the regolith geometry, and, in particular, its thickness, which, in turn, is controlled by the velocity of the fluid.

To study these couplings and potential feedbacks, we have first solved the two coupled equations ((6) and (11)) numerically for a system (or hill) of lateral dimension L, surface slope, S, and zero initial regolith thickness. We arbitrarily assume that $L = 1000$ m, $S = 0.01$, $P_0 = 1$ m/yr, $K = 10^4$ m/yr, and $F = 10^{-6}$. In Figure 4a, we show the solution at three time steps in the system evolution. Initially, the aquifer is so thin that it is fully saturated and the surface of the water table follows the surface topography. Progressively, the regolith layer thickens and the regolith in the upper part of the hill becomes unsaturated. The first of the three time panels shown in Figure 4a corresponds to the time where the surface of the water table intersects the surface at $x = L/2$. For the specific parameter values given above, this time corresponds to 50 kyr.

In the unsaturated section, the surface of the water table is concave (the slope decreases with increasing x), and consequently, the rate of propagation of the weathering front decreases with increasing x. This produces curvature in the weathering front, and as time progresses (second and third panels in Figure 4a) a regolith profile thickens toward the base of the hill. Note that the regolith thickness keeps increasing with time (there is no steady state solution), but the rate of propagation decreases as time increases (circles in Figure 4c).

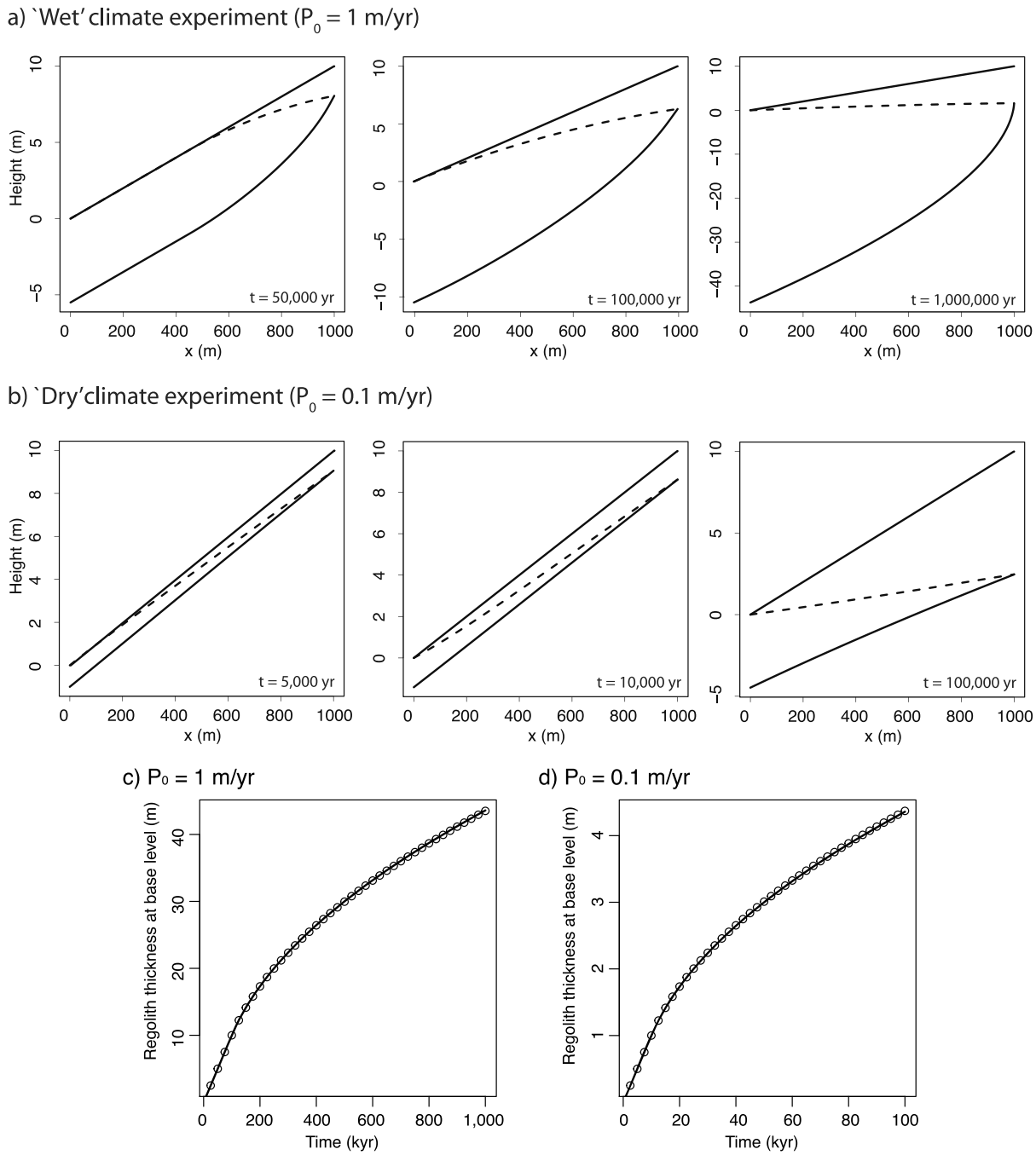


Figure 4. Numerical solutions of the coupled hydrological and weathering front evolution equations. Note that vertical scale is different in each panel. Parameter values are given in the text. (a) Three times steps in the model evolution for a precipitation rate of $P_0 = 1$ mm/yr. (b) Similar points in the system evolution when $P_0 = 0.1$ m/yr. The top and bottom black lines are the surface (z) and the weathering front ($z - B$), respectively; the dashed line is the surface of the water table (H). (c, d) The corresponding computed time evolution of the regolith thickness at the base of the hill, $B_s(x = 0)$, for $P_0 = 1$ and 0.1 m/yr, respectively.

In a second numerical experiment (Figure 4b), we used a precipitation (or more exactly infiltration) rate of 0.1 m/yr corresponding to a drier climate. The solution is also shown at the same "instants" in the evolution of the system, i.e., when the water table intersects the surface at midslope (first panel of Figure 4b), when it intersects the base of the hill (second panel of Figure 4b), and much later (third panel of Figure 4b). With the reduced precipitation rate, it only takes 5 kyr for the surface of the water table to intersect the surface at midheight, because this stage in the evolution of the system is achieved for much smaller soil thickness (approximately one tenth). At this point in time, the surface of the water table is convex (the slope increases

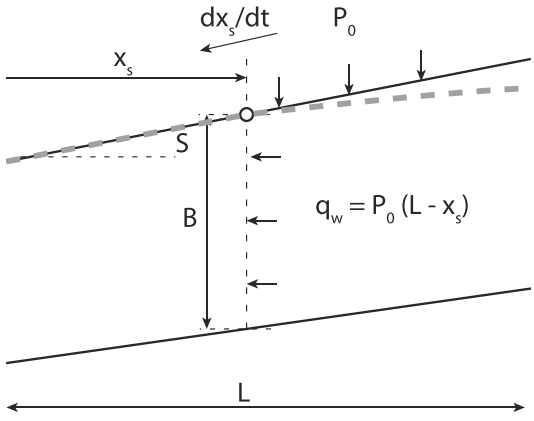


Figure 5. Sketch illustrating the propagation of the point, x_s, where the surface of the water table (thick dashed grey line) intersects the topographic surface. q_w is the integral of precipitation upstream of x_s which must be equal to the flow of water through the regolith of thickness B at a velocity given by the product of the surface slope, S, and the hydraulic conductivity K.

with increasing x), and consequently, the rate of propagation of the weathering front increases with increasing x. As time progresses, this produces a large regolith thickness beneath the top of the hill. Again, the system does not reach steady state but its rate of evolution decreases with time (circles in Figure 4d).

4.1. Propagation of the Saturation Point

To understand these results, we will now derive an analytical expression for the thickness of the regolith at the base of the hill and the time it takes to develop that thickness. To do this, we first consider how the weathering front propagates on either side of the transition point separating fully saturated from unsaturated conditions, which we will call the *saturation point*. Under saturated conditions, i.e., below the saturation point, the rate of regolith thickening is proportional to surface slope; under unsaturated conditions, i.e., above the saturation point, the water table is disconnected from the surface and the rate of regolith thickening is proportional to the slope of the water table.

We introduce, x_s, the position of the saturation point, which is the intersection of the water table with the surface topography. At the point x_s the system is at the transition between saturated and unsaturated conditions (Figure 5) such that the flux of water through the regolith column of thickness $B(x_s)$ must be exactly equal to the uphill integrated rainfall

$$KSB = P_0(L - x_s) \tag{23}$$

The rate of downhill propagation of x_s is therefore given by

$$\frac{\partial x_s}{\partial t} = -\frac{KS}{P_0}\frac{\partial B}{\partial t} \tag{24}$$

The minus sign simply indicates that the saturation point is propagating from right to left, i.e., in the direction of decreasing x. Under saturated conditions, i.e., downhill of x_s, the rate of vertical propagation of the weathering front is given by

$$\frac{\partial B}{\partial t} = FKS \tag{25}$$

where S is surface slope. Combining the two, we obtain

$$\frac{\partial x_s}{\partial t} = -\frac{FK^2S^2}{P_0} \tag{26}$$

from which we can derive the time it takes for a hill of length L to evolve from fully saturated to fully unsaturated conditions in response to regolith thickening by weathering

$$\tau_s = -L/\frac{\partial x_s}{\partial t} = \frac{LP_0}{FK^2S^2} \tag{27}$$

We note that this time is linearly proportional to the precipitation rate but inversely proportional to the square of the slope and the hydraulic conductivity. Consequently, for a given lithology and weathering process (i.e., a given value of K and F), we see that the rate of regolith formation is primarily controlled by the surface slope, S, and, to a lesser degree by the climate (precipitation rate, P_0) and the size of the relief, L. In Figure 6a, we show how this characteristic time of evolution from saturated to unsaturated conditions for $L = 1000$ m, $F = 10^{-6}$, and $K = 10^4$ m/yr, as a function of precipitation rate, P_0, and slope, S.

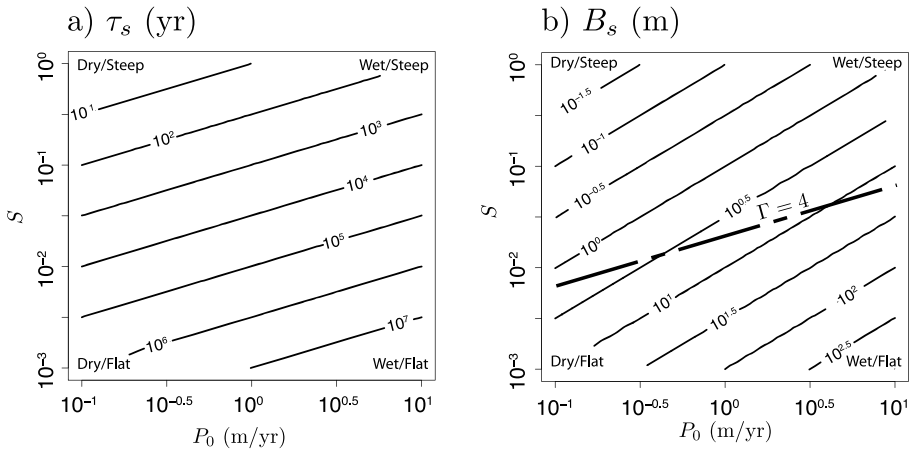


Figure 6. (a) Contours of the logarithm of the characteristic timescale, τ_s in years, for evolution from saturated to unsaturated conditions and (b) contours of the logarithm of the typical regolith thickness, B_s in meters, for a hill of length $L = 1000$ m. $F = 10^{-6}$ and $K = 10^4$ m/yr and F are assumed. Both τ_s and B_s values should be multiplied by 10 for a 10 km long hill and divided by 10 for 100 m long hill. Thick dashed line corresponds to values of P_0 and S such that $\Gamma = 4$. For values of P_0, S above the line $\Gamma = 4$, the regolith layer grows thicker under the summit; below the line $\Gamma = 4$, the regolith layer grows thicker at the base of the hill, i.e., near base level.

During the transformation from fully saturated conditions to fully unsaturated conditions, the rate of propagation of the weathering front has remained constant at the base of the hill (x=0) and equal to FKS. Multiplying this rate by τ_s gives the thickness of the regolith layer at the base of the hill at time τ_s

$$B_s = FKS\tau_s = FKS\frac{LP_0}{FK^2S^2} = \frac{LP_0}{KS} \tag{28}$$

Interestingly, this regolith length scale or "typical regolith thickness" is independent of F, the weathering rate constant. It increases with precipitation rate and the length of the system but decreases with the effective regolith hydraulic conductivity and the surface slope. In Figure 6b, we show contours of B_s as a function of surface slope and precipitation rate, for $L = 1000$ m, $F = 10^{-6}$, and $K = 10^4$ m/yr.

4.2. Propagation of the Weathering Front Under Unsaturated Conditions

When the surface of the water table has reached base level, i.e., at $t = \tau_s$, we can write by applying equation (6) at the point $x = 0$ where $z = H$

$$KBS_H = P_0L \tag{29}$$

where S_H is the slope of the surface of the water table at $x = 0$. Combining this with the evolution equation for B at $x = 0$,

$$\frac{\partial B}{\partial t} = FKS_H \tag{30}$$

gives

$$\frac{\partial B}{\partial t} = \frac{FP_0L}{B} \tag{31}$$

which is a simple differential equation for B having the following solution:

$$B = \sqrt{2FP_0Lt + B_s^2} \tag{32}$$

assuming that $B(t = 0) = B_s$. This shows that, after the hill has become unsaturated, the weathering front deepens as the square root of time. This explains why in both numerical experiments (Figure 4), the system does not reach steady state and why the rate of regolith thickening decreases with time.

In Figures 4b and 4c, we plotted, as thick lines, the regolith thickness at the base of the hill, $B(x = 0)$, obtained from these analytical solutions, i.e., $B = B_s t/\tau_s$ for $t < \tau_s$ and equation (32) for $t > \tau_s$. These analytical expressions agree with the numerical solutions, within numerical accuracy.

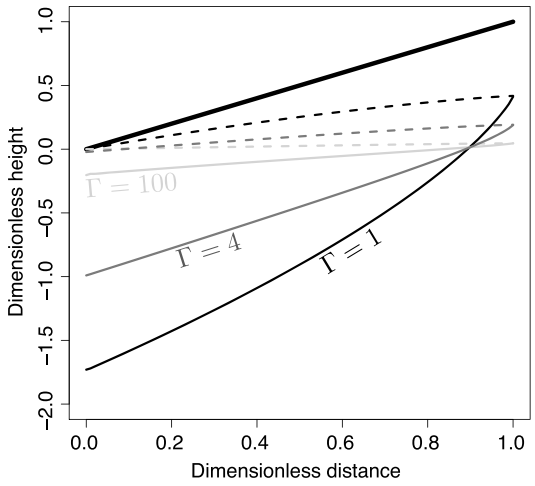


Figure 7. Dimensionless position of the weathering front (solid lines) and water table (dashed lines) as a function of dimensionless position along the hill for sets of model parameter values corresponding to different values of the dimensionless parameter Γ (black line corresponds to $\Gamma = 1$, dark grey corresponds to $\Gamma = 10$, and light grey corresponds to $\Gamma = 100$). All solutions are shown at $t = 10\ \tau_s$. Distance (horizontal axis) is scaled by L, and height (vertical axis) is scaled by the height of the hill LS. Thick black line at top is surface topography.

4.3. Dimensionless Number and Regolith Geometry

A simple dimensionless number, which we term Γ, can be derived by dividing the product of the slope, S, by the horizontal rate of propagation of the saturation point, x_s, i.e., $\frac{\partial x_s}{\partial t}$, by the vertical rate of propagation of the weathering front, $\frac{\partial B}{\partial t} = FKS$, during the transition from saturated to unsaturated conditions

$$\Gamma = S\frac{\partial x}{\partial t}/\frac{\partial B}{\partial t} = \frac{KS^2}{P_0} \tag{33}$$

The slope S must be introduced to properly compare the *vertical* rate of weathering front propagation with the *horizontal* rate of propagation of the saturation point, x_s.

If the rate of propagation of x_s is rapid compared to the weathering rate at the base of the hill ($\Gamma \gg 1$), the regolith profile will be thinnest at the base of the hill; conversely, if the rate of propagation of x_s is slow compared to the weathering rate at the base of the hill ($\Gamma \ll 1$), the regolith profile will be thickest at the base of the hill. This is confirmed by the numerical model: in Figure 7 we show a series of curves representing the computed shape (thickness) of the regolith layer at time $t = 10 \times \tau_s$ for different values of Γ. In this figure we used dimensionless variables to represent the solution, i.e., x/L along the horizontal axis and $z/(LS)$ along the vertical axis. This allows to compare solutions in terms of the shape of the predicted regolith profile, not its absolute thickness. The results show that by using Γ we can easily define the regions of parameter space corresponding to two different behaviors. For values of Γ larger than 4, the rate of propagation of the saturation point is larger than the propagation of the weathering front and the regolith thickness is uniform at time τ_s and the surface of the water table is convex. Further evolution leads therefore to faster regolith thickening at high elevation, i.e., near the summit of the hill, as shown in Figure 7 (curves labeled $\Gamma = 4$ and 100). For values of Γ smaller than 4, the weathering front propagates significantly downward during the propagation of the saturation point. The resulting regolith profile has consequently developed a finite curvature by the end of the propagation of the saturation point and is also thicker at the base of the hill. The surface of the water table is concave, and further propagation of the weathering profile leads to preferential thickening of the regolith profile at the base of the hill, as shown in Figure 7 (curve labeled $\Gamma = 1$). Thus, the condition that determines the distribution of the regolith, i.e., whether it is thickest at the top or at the bottom of the hill, is as follows:

$$\Gamma = \frac{KS^2}{P_0} \gtrless 4 \tag{34}$$

This leads to one of the main results/predictions of our model in anorogenic areas: if our assumption that the propagation of the weathering front is linearly related to the velocity of the fluid at the base of the regolith layer is valid, we predict that the distribution of regolith beneath a hill of slope S is controlled by the value of a single dimensionless number, $\Gamma = KS^2/P_0$, which combines the slope of the hill, the precipitation rate, and the hydraulic conductivity of the regolith. Γ is, however, independent of the value of the weathering rate constant, F, that relates the rate of propagation of the weathering front to the fluid velocity. We note that in the expression for Γ, the slope dependence is dominant, i.e., doubling the slope is equivalent to decreasing precipitation by a factor of 4.

It is also worth noting that Γ can be expressed as a ratio of timescales as follows:

$$\Gamma = \frac{\tau}{\tau_s} = \frac{L/FK}{LP_0/FK^2S^2} = \frac{KS^2}{P_0} \tag{35}$$

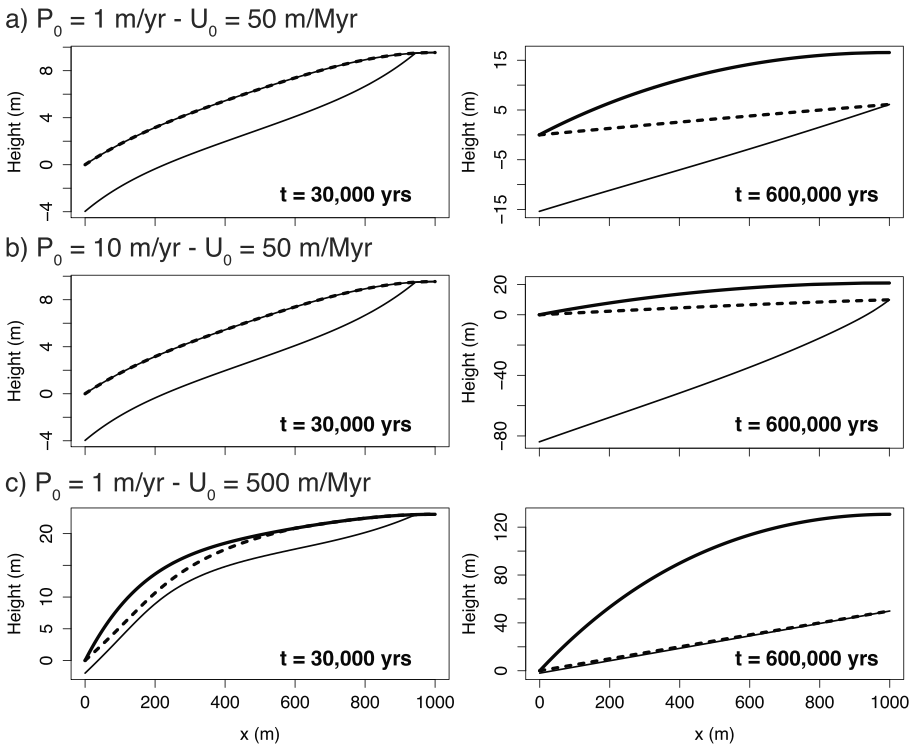


Figure 8. Predicted topography (thick solid line), water table (thick dashed line), and weathering front or base of the regolith layer (thin solid line) for three different model runs corresponding to (a) $P_0 = 1$ m/yr and $U_0 = 50$ m/Myr, (b) $P_0 = 10$ m/yr and $U_0 = 50$ m/Myr, and (c) $P_0 = 1$ m/yr and $U_0 = 500$ m/Myr. Figure 8 (left column) corresponds to the time step where system evolves from fully saturated to unsaturated conditions, and Figure 8 (right column) corresponds to the steady state solution.

where τ is the time necessary to propagate the weathering front to a depth equal to the height of the hill, $z_t = LS$, under saturated conditions, i.e., at a rate FKS. It can also be expressed as a ratio of the height of the hill, z_t, to the thickness of regolith formed at the base of the hill under saturated conditions, B_s

$$\Gamma = \frac{z_t}{B_s} = \frac{LS}{LP_0/KS} = \frac{KS^2}{P_0} \tag{36}$$

That a dimensionless number can be expressed as a ratio of heights means that its value can be directly measured in the field, without having to measure or guess the value of poorly constrained physical parameters such as K. Timescales are also very useful descriptors of the behavior of a system in that they provide estimates on how fast a system responds to changes in forcing or in environmental conditions. Consequently, a simple, yet powerful application of our model, and the dimensionless number we extracted from it, is to derive a ratio of timescales from a ratio of length scales, directly measurable in the field. In section 6.5, we provide an example on how this can be done, using a well-documented example from India.

Finally, if one considers the natural range of values for K ($10^3 - 10^5$ m/yr), P_0 ($10^{-1} - 10^1$ m/yr), and S ($10^{-3} - 10^0$) among regolith-mantle hillslopes, we find that expected values for Γ are in the range ($10^{-4} - 10^6$), which implies that both behaviors are expected to be observed in natural systems.

5. Model Behavior in Orogenic Areas

5.1. Solutions With Constant Uplift Rate and Surface Erosion

We now turn our attention to situations where the landscape is dynamically supported by tectonic uplift, at a rate U_0. In Figure 8, we show the time evolution of the system, assuming unit erosional efficiency (or diffusivity or transport coefficient) $K_D = 1$ m^2/yr. Three runs are presented corresponding to (Figure 8a) $P_0 = 1$ m/yr and $U_0 = 50$ m/Myr, (Figure 8b) $P_0 = 10$ m/yr and $U_0 = 50$ m/Myr, and (Figure 8c) $P_0 = 1$ m/yr and $U_0 = 500$ m/Myr. These values are selected to illustrate the sensitivity of the model; they are not meant to

represent any specific location but fall within the range of observed values. The first important difference with the solution for anorogenic areas (U_0=0) is that the system tends toward a steady state. For all three runs, we present the solution at or around the time the system evolves from fully saturated to unsaturated conditions (left column in Figure 8) and at steady state (right column in Figure 8).

The second point of interest is that the unsaturated conditions evolve from the base of the hill toward the top and that, when this transition takes place, the regolith thickness is almost uniform.

The third point of interest is that depending on the value of P_0 and U_0, predicted steady state regolith can be thickest under the base of the hill or thickest near the summit. For high precipitation rate and/or slow uplift rate, the regolith is thickest near the base of the hill; for low precipitation rate and/or fast uplift rate, the regolith is thickest at the top of the hill. Note that higher uplift rates correspond to steeper surface slopes. This is because we use the same value for the transport coefficient, K_D, in all models. Note also that we have not connected the efficiency of surface erosion/transport to precipitation implying that varying precipitation rate affects the hydrological model but not the surface erosion model.

Finally, we note that, for all parameter values, the steady state solution tends toward a concave surface topography, a linear water table and that, at the top of the hill, the weathering front coincides with the water table, i.e., $H = z - B$ at $x = L$.

In order to understand the behavior of this system, we are now going to study the shape of the steady state solution, as well as characteristics timescales during the transition toward steady state.

5.2. Steady State Topography

The steady state surface topography, i.e., at equilibrium between tectonic uplift and surface erosion/transport ($\frac{\partial z}{\partial t} = 0$ in equation (21)) is given by

$$z = -\frac{U_0}{2K_D}x^2 + \frac{U_0 L}{K_D}x \tag{37}$$

and the steady state surface slope, $S(x)$, by

$$S(x) = \frac{\partial z}{\partial x} = \frac{U_0}{K_D}(L - x) \tag{38}$$

5.3. Condition for the Existence of a Regolith Profile

Under fully saturated conditions, the rate of weathering front propagation is proportional to surface slope and is therefore highest where surface slope is highest, i.e., at the base of the hill ($x = 0$). Assuming topographic steady state and an imposed uplift rate U_0, the rate of thickening of the regolith profile at $x = 0$ is given by

$$\frac{\partial B}{\partial t} = FKS(x = 0) - U_0 = FK\frac{U_0 L}{K_D} - U_0 = U_0\left(\frac{FKL}{K_D} - 1\right) \tag{39}$$

For a regolith profile to exist at the base of the hill, and consequently anywhere else on the hill, this rate needs to be greater than zero, which implies that

$$\frac{FKL}{K_D} > 1 \tag{40}$$

This condition depends on the hill length, L, and rock properties, F, K, and K_D.

5.4. Steady State Weathering Front

To reach steady state regolith thickness, the weathering front must propagate at a velocity that is equal to the erosion rate at every point along the hill, which, in the case of topographic steady state, is also equal to the uplift rate, U_0. This condition can be expressed as follows:

$$\frac{\partial B}{\partial t} = FK\frac{\partial H}{\partial x} - U_0 = 0 \tag{41}$$

which leads to a simple equation for the steady state water table surface, H

$$H(x) = \frac{U_0 x}{FK} \tag{42}$$

if we assume that the water table is at the surface at the base of the hill ($H(x=0)=0$). This equation implies that, at steady state, the water table surface must be planar and its slope given by $U_0/(FK)$.

5.5. Condition for Regolith at the Top of the Hill

The existence of a steady state finite regolith thickness at the top of the hill requires that the surface of the water table at the top of the hill, H_t, be lower than the surface of the hill, z_t; otherwise, the water table slope and the rate of weathering front propagation is controlled by the slope of the hill, which is nil at the top of the hill. This implies that

$$z_t - H_t = \frac{U_0 L^2}{2K_D} - \frac{U_0 L}{FK} = \frac{U_0 L}{FK}\left(\frac{FKL}{2K_D} - 1\right) > 0 \tag{43}$$

This condition is fulfilled when

$$\Omega = \frac{FKL}{2K_D} > 1 \tag{44}$$

The value of the dimensionless number Ω therefore controls whether there will be any regolith along the hill ($\Omega > 1/2$ from equation (40)) and also whether, at steady state, the entire hill is covered by a weathering profile ($\Omega > 1$).

We can also assume that the steady state regolith thickness at the top of the hill, B_t, will be equal to the depth of the water table

$$B_t = z_t - H_t = \frac{U_0 L}{FK}(\Omega - 1) = \frac{z_t}{\Omega}(\Omega - 1) = z_t\left(1 - \frac{1}{\Omega}\right) \tag{45}$$

and the relative regolith thickness, i.e., normalized by the hill height, is

$$B_t/z_t = \frac{z_t - H_t}{z_t} = 1 - \frac{1}{\Omega} \tag{46}$$

which varies between 0 and 1 as Ω goes from 1 to ∞, which implies that the maximum regolith thickness that can be achieved at the top of the hill is the height of the hill (i.e., when $\Omega \to \infty$). This also implies that the value of the dimensionless number Ω can be directly measured from the relative steady state regolith thickness at the top of the hill

$$\Omega = \frac{1}{1 - B_t/z_t} \tag{47}$$

Ω is also the ratio between the steady state mean surface slope (hill height divided by hill length), $\bar{S} = U_0 L/2K_D$, and the water table slope, S_H

$$\Omega = \frac{\bar{S}}{S_H} \tag{48}$$

because according to equation (42)

$$S_H = \frac{U_0}{FK} = \frac{2\bar{S}K_D}{FKL} = \frac{\bar{S}}{\Omega} \tag{49}$$

Equation (47) or (48), shows that although B_t and z_t (or S_H and $\bar{S}$) depend on the uplift rate, U_0, their ratio and thus Ω do not.

5.6. Geometry of the Regolith

From the slope of the water table, we can deduce the steady state flow velocity, $v = KS_H$. At the base of the hill ($x=0$), the water table coincides with the surface topography, and the total water flux, given by

$$vB_b = \frac{KU_0 B_b}{FK} = \frac{U_0 B_b}{F} \tag{50}$$

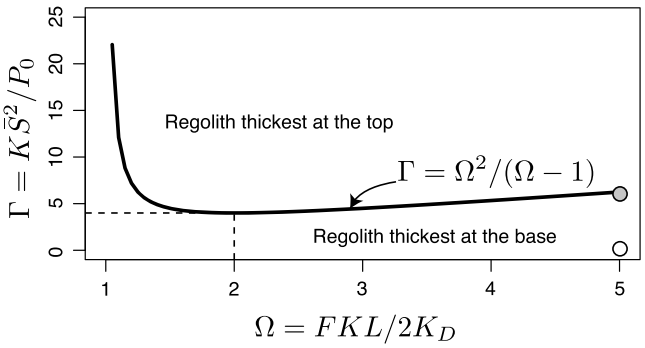


Figure 9. Critical value for the dimensionless number $\Gamma = K\bar{S}^2/P_0$, as a function of $\Omega = FKL/2K_D$. The two circles correspond to the positions of the model runs shown in Figures 8a and 8b.

must be equal to the integrated precipitation, P_0L. B_b is the thickness of the regolith layer at the base of the hill. This gives the following expression for B_b

$$B_b = \frac{FP_0L}{U_0} \tag{51}$$

The ratio B_t/B_b is a first-order measure of the geometry of the steady state regolith profile; it can be written as follows:

$$\frac{B_t}{B_b} = \frac{U_0L}{FK}(\Omega - 1)/\frac{FP_0L}{U_0} = \frac{U_0^2L}{F^2KP_OL}(\Omega - 1) = \frac{K\bar{S}^2}{P_0}\frac{4K_D^2}{F^2K^2L^2}(\Omega - 1) = \Gamma\frac{\Omega - 1}{\Omega^2} \tag{52}$$

where, in this case,

$$\Gamma = \frac{K\bar{S}^2}{P_0} \tag{53}$$

From this relationship, we see that the steady state geometry of the regolith (i.e., whether it is thicker under the summit or the base of the hill) is also controlled by the value of the dimensionless number, Γ, defined here using the mean slope of the hill, $\bar{S}$, in place of S, the "true" slope of the hill in the anorogenic case. The condition that determines the geometry of the regolith, i.e., whether it is thickest at the base or at the top of the hill, becomes

$$\Gamma \gtrless \frac{\Omega^2}{\Omega - 1} \tag{54}$$

In Figure 9, we show this critical value for Γ $(= \Omega^2/(\Omega - 1))$ as a function of Ω. We see that for values of Ω close to 1 (left-hand side of the diagram), the critical value is very large (it tends to ∞ as Ω tends to 1) and the condition for the thickest regolith at the base of the hill, namely, $\Gamma < \Omega^2/(\Omega - 1)$, is almost always achieved, even for high values of the uplift rate (and thus high surface slope). The critical value reaches a minimum (=4) for $\Omega = 2$, which, according to equation (47), corresponds to $B_t = z_t/2$. At this critical value, the condition for relative regolith thickness between top and bottom of the hill is identical to that we derived for the anorogenic case (equation (34)). For values of $\Omega > 2$, the critical value increases almost linearly as follows:

$$\lim_{\Omega >> 2} \frac{\Omega^2}{\Omega - 1} \approx \Omega \tag{55}$$

and the situation where the regolith is thickest at the base of the hill is achieved for progressively larger values of the uplift rate (or surface slope equivalent).

In Figure 9, we also show the "position" of the model runs shown in Figures 8a and 8b. For both model runs, $\Omega = 5$. For the first model (grey circle) $\Gamma = 6.25$ and the model sits exactly on the line $\Gamma = \Omega^2/(\Omega - 1)$, which explains why regolith thickness is uniform (Figure 8a); for the second model (white circle) $\Gamma = 0.625$ and the model sits well below the line $\Gamma = \Omega^2/(\Omega - 1)$, which explains why regolith is thicker near the base of the hill (Figure 8b). The model run shown in Figure 8c has a value of $\Gamma = 625$ (largely off scale in Figure 9), which explains why predicted regolith thickness is thicker beneath the summit of the hill.

Finally, we note that the thickness of regolith at the base of the hill, B_b, can also be expressed as a fraction of the hill height, z_t, according to

$$B_b = z_t \frac{\Omega}{\Gamma} \tag{56}$$

and the value of the dimensionless number Γ can be obtained according to

$$\Gamma = \Omega\,(z_t/B_b) \tag{57}$$

from the relative thickness of the regolith at the base of the hill, i.e., normalized by the hill height, and Ω, which can be directly obtained from the relative thickness of the regolith at the top of the hill (equation (46)).

5.7. Timescales

During the transition from fully saturated to unsaturated conditions, we can write that, at the point x_s where the water table intersects the surface topography, the flux of water through the regolith (of thickness B_s^*) must be equal to the integrated precipitation rate

$$B_s^* KS(x_s) = B_s^* K \frac{U_0}{K_D}(L - x_s) = P_0(L - x_s) \tag{58}$$

which gives

$$B_s^* = \frac{P_0 K_D}{K U_0} = \frac{L P_0}{2K\bar{S}} \tag{59}$$

This implies that the transition from saturated to unsaturated conditions takes place for the same regolith thickness at all points of the hill. B_s^* can be seen as the typical regolith thickness at the transition between saturated and unsaturated flows.

Under saturated conditions, the rate of regolith formation at the base of the hill is proportional to surface slope, $S_b = U_0 L/K_D$, according to

$$\frac{\partial B}{\partial t} = FKS_b = 2FK\bar{S} \tag{60}$$

and the time required to achieve unsaturated conditions at the base of the hill is

$$\tau_s^* = B_s^* / \frac{\partial B}{\partial t} = \frac{P_0 K_D}{2FK^2 U_0 \bar{S}} = \frac{P_0 L}{4FK^2 \bar{S}^2} = \frac{P_0 L}{FK^2 S_b^2} \tag{61}$$

This expression is identical to that derived in the anorogenic case (equation (27)), except that the assumed constant hill slope S has been replaced by the slope at the base of the hill, S_b.

Let us now consider the time it takes to approach steady state regolith thickness at the top of the hill, i.e., B_t. We will assume that during the formation of the regolith layer, the average slope of the water table is equal to the surface slope in the middle of the hill (at $x = L/2$). The corresponding rate of regolith thickening is

$$\frac{\partial B}{\partial t} = FK \frac{U_0}{K_D}(L - L/2) - U_0 = U_0(\Omega - 1) \tag{62}$$

The time required to approach regolith steady state thickness, $B_t = \frac{U_0 L}{FK}(\Omega - 1)$, at that rate is given by

$$\tau^* = B_t / \frac{\partial B}{\partial t} = \frac{L}{FK} \frac{\Omega - 1}{\Omega - 1} = \frac{L}{FK} \tag{63}$$

This is the characteristic weathering time of the system. Interestingly, it has the same expression as, τ, the timescale necessary to develop a regolith of thickness $S \times L$ in anorogenic areas (cf. equation (35)).

At this point, we note that the dimensionless number Ω can also be expressed as the ratio of two characteristic timescales

$$\Omega = \tau_e / \tau^* = \frac{L^2/2K_D}{L/FK} = \frac{FKL}{2K_D} \tag{64}$$

where $\tau_e = L^2/2K_D$ is the erosion or diffusion timescale, i.e., the characteristic time for surface erosion/transport to transform a hill of dimension L into its steady state shape given by equation (37). This means that the condition for the existence of a regolith layer in an actively uplifting and eroding region ($\Omega > 1$) is that the erosional timescale be larger than the weathering timescale

$$\tau_e > \tau^* \tag{65}$$

From this, we also note that Ω is in fact very similar to the second or erosional Damköhler number, Da_r, which is defined as the ratio of the timescale for the advection of rocks through the regolith profile (by tectonic uplift and erosion) to the timescale for weathering of the same profile [*Lebedeva et al.*, 2007; *Hilley et al.*, 2010; *Li et al.*, 2014].

Similarly, the dimensionless number Γ is, as in anorogenic systems, proportional to the ratio of the weathering timescale, τ^*, to the timescale necessary to reach unsaturated conditions, τ_s^*

$$\Gamma = \frac{\tau^*}{4\tau_s^*} = \frac{L}{FK} \Big/ \frac{4P_0 L}{FK^2 S_b^2} = \frac{K\bar{S}^2}{P_0} \tag{66}$$

5.8. Steady State Regolith Profile Under an Arbitrary Surface Topography

We have shown that for regolith to exist at the surface of a hill, the dimensionless number Ω must be larger than 1, which is equivalent to say that the weathering response time has to be smaller than the erosional response time. In other words, making the assumption that surface erosion is at steady state with tectonic uplift implies that the system has also reached weathering steady state. This leads us to now develop and present a generalized steady state solution for the geometry of regolith beneath a hill of arbitrary geometry.

Under an arbitrary surface topography, $z(x)$, the water table geometry, $H(x)$, obeys

$$(H - z + B)\, K \frac{\partial H}{\partial x} = P_0 (L - x) \tag{67}$$

Assuming weathering steady state

$$\frac{\partial B}{\partial t} = FK \frac{\partial H}{\partial x} - \dot{\epsilon} = 0 \tag{68}$$

leads to

$$H^a(x) = H^a(0) + \frac{\dot{\epsilon}}{FK} x = \frac{\dot{\epsilon}}{FK} x \tag{69}$$

where the superscript a stands for "arbitrary," in reference to the arbitrary geometry of the assumed surface topography, and, consequently, to the generality of this solution. Combining these three relationships leads to the following:

$$B^a(x) = \frac{P_0 (L - x)}{K(\partial H/\partial x)} + z(x) - H^a(x) = z(x) + \frac{FP_0}{\dot{\epsilon}} (L - x) - \frac{\dot{\epsilon}}{FK} x \tag{70}$$

from which the steady state regolith thicknesses at the base of the hill, B_b^a, and the top of the hill, B_t^a, can be derived as follows:

$$B_b^a = \frac{FP_0 L}{\dot{\epsilon}} \quad \text{and} \quad B_t^a = z_t - \frac{\dot{\epsilon} L}{FK} \tag{71}$$

These expressions lead, in turn, to general expressions for the dimensionless parameters, Ω and Γ, as a function of $\bar{S}$, the mean slope of the arbitrary topography

$$\Omega = \frac{FK\bar{S}}{\dot{\epsilon}} \quad \text{and} \quad \Gamma = \frac{K\bar{S}^2}{P_0}, \quad \text{where} \quad \bar{S} = \frac{z_t}{L} \tag{72}$$

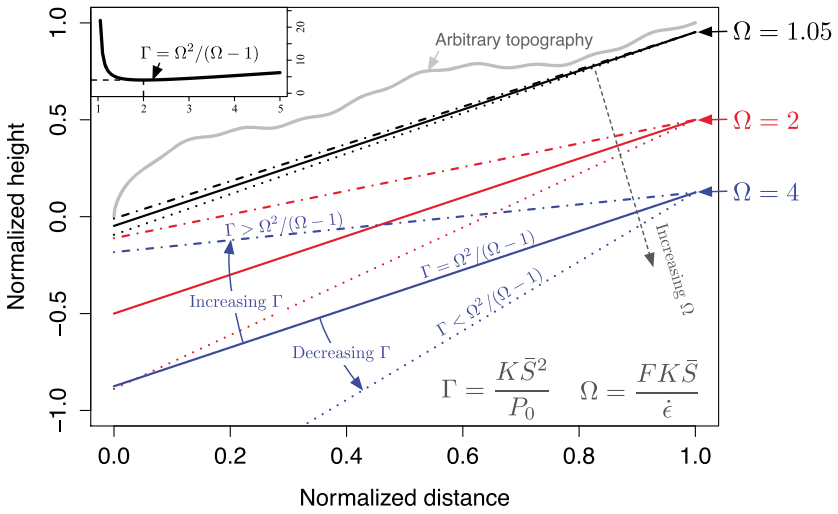


Figure 10. Predicted steady state regolith geometries for an arbitrary surface geometry (thick grey line). Solid lines correspond to cases where $\Gamma = \Omega^2/(\Omega - 1)$ for three different values of Ω: 1.05 (black), 2 (red), and 4 (blue). The dotted (dashed) lines correspond to a value of Γ that is smaller (greater) than $\Gamma = \Omega^2/(\Omega - 1)$.

which can be used to predict the distribution of regolith thickness beneath the arbitrary topography, $z(x)$, through the following generalized condition:

$$\Gamma \gtrless \frac{\Omega^2}{\Omega - 1} \tag{73}$$

as

$$\frac{B_t^a}{B_b^a} = \Gamma \frac{\Omega - 1}{\Omega^2} \tag{74}$$

The value of Ω can be directly measured from the steady state, relative regolith thickness at the top of the arbitrary topography

$$\Omega = \frac{1}{1 - B_t^a/z_t} \tag{75}$$

and the value of Γ from the steady state, relative regolith thickness at the base of the arbitrary topography

$$\Gamma = \Omega\,(z_t/B_b^a) \tag{76}$$

Finally, we note that the normalized steady state regolith thickness can be expressed in terms of the two dimensionless numbers, Ω and Γ

$$\frac{B^a(x)}{z_t} = \frac{z(x)}{z_t} + \frac{\Omega}{\Gamma}\,(1 - x/L) - \frac{1}{\Omega}\,(x/L) \tag{77}$$

which also provides expressions for the normalized regolith thickness at the bottom and top of a hill of arbitrary surface geometry

$$\frac{B_b^a}{z_t} = \frac{\Omega}{\Gamma} \quad \text{and} \quad \frac{B_t^a}{z_t} = 1 - \frac{1}{\Omega} \tag{78}$$

In Figure 10, we show how the predicted normalized regolith thickness varies with the two dimensionless numbers. The thick grey line represents the arbitrary surface topography, while all other lines are steady state solutions for the base of the regolith layer (the weathering front). When $\Gamma = \Omega^2/(\Omega - 1)$, the regolith has a uniform thickness (solid lines) which only depends on the value of Ω, given by

$$\frac{B_b^a}{z_t} = \frac{B_t^a}{z_t} = 1 - \frac{1}{\Omega} \tag{79}$$

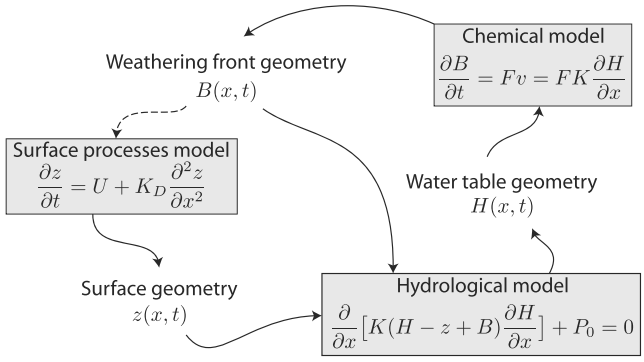


Figure 11. Connectivity between the three components of the new model we have developed. The hydrological model predicts the geometry of the water table, $H(x)$, which is used to drive the propagation of the weathering front. The surface processes model predicts the surface geometry, $z(x)$, which, in combination with the thickness of the regolith layer, $B(x)$, is used to define the geometry of the aquifer in the hydrological model. The surface processes model only applies where there is a finite regolith thickness, implying a weak control of the weathering front geometry on the surface processes model (dashed arrow).

For a given value of Ω, varying Γ changes the thickness at the base of the hill and thus the distribution of the regolith. Decreasing Γ (dotted lines) causes the regolith to become thinner at the base of the hill, while increasing Γ (dashed lines) causes the regolith to become thinner at the base of the hill.

From equation (72), we see that, for a given lithology (i.e., given values of F and K), Ω is a function of erosion rate, $\dot{\epsilon}$, and mean surface slope, $\bar{S} = z_t/L$: the faster the erosion, or the steeper the surface slope, the lower Ω and the thinner the regolith layer. Γ is, for a given lithology, a function of slope, $\bar{S}$, and precipitation rate, P_0: the steeper the surface slope, or the lower the precipitation rate, the thinner the regolith will be at the base of the hill.

6. Discussion

6.1. The Model as a Coupled System

We have constructed a new model to predict the formation of regolith by downward propagation of a chemical weathering front by bringing together three simple components as shown in Figure 11. These are the following:

1. A hydrological model based on the assumption of a uniform hydraulic conductivity, uniform precipitation rate (or infiltration rate), and steady state conditions; the aquifer is bounded by the surface and the weathering front computed in 2 and 3, respectively.
2. A surface process model based on slope-proportional transport of the regolith (or the soil layer derived from it) to compute surface topography evolution.
3. A chemical weathering model that assumes that propagation of the weathering front is linearly related to the velocity of the fluid and thus to the slope of the water table computed in 1 or the surface slope computed in 2, depending on saturation.

The system is strongly coupled and displays a behavior that involves strong feedbacks. The hydrological model is at the core of these interactions as the water table geometry is a strong function of the geometry of the regolith layer (bounded at the top by the surface model and at the base by the weathering model) and controls the evolution of the weathering front.

6.2. Model Hypotheses, Assumptions, and Simplifications

First, in developing this new model, we have made choices concerning the processes at play, which need to be discussed here. Conceptually, the model assumes that the weathering process is solely controlled by the propagation of a dissolution front. Where fracturing or other nonchemical processes are known to dominate weathering, one should not expect that the behavior of the model we present here be applicable. Similarly, we have assumed that the dominant surface process is hillslope transport. This has helped in parameterizing surface processes with a minimal parameter set (K_D, the transport coefficient). In Figure 12 we present results of a model in which transport is assumed to be nonlinear both with respect to slope and soil thickness (equation (19)). The solution is shown at steady state for two values of the uplift rate ($U_0 = 50$ and 500 m/Myr)

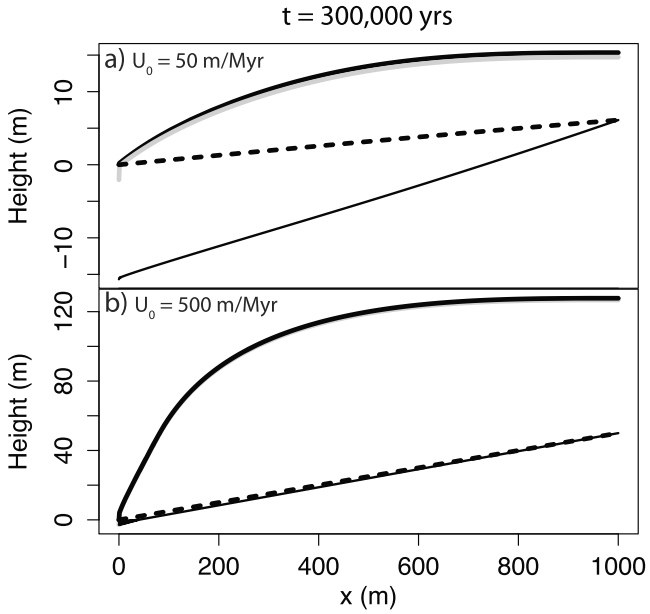


Figure 12. Model results obtained using the nonlinear surface processes model described by equation (19). The basic behavior of thinner regolith near the summit for (a) low uplift rate and thinner regolith thickness near the base for (b) high uplift rate is observed. Thick solid black line is surface topography (z), thick solid grey line is base of mobile soil layer ($z - D$), thick dashed black line is surface of the water table (H), and the thin solid black line is the base of the regolith layer ($z - B$).

and demonstrates that the behavior of the system (strong dependence of the regolith geometry on uplift rate and surface slope) is independent of the assumed surface process formulation or parameterization. We have further demonstrated this very important point by deriving an analytical solution for the steady state of the system under an arbitrary surface topography (see section 5.8).

Second, we need to review the assumptions we have made in developing the parameterization of these processes. Several of these assumptions are driven by the need to integrate the equations over long, geological timescales, which requires and also justifies the quasi steady state approximation (i.e., neglecting inertial effects) for all three physical processes at play (surface erosion and transport, chemical dissolution, and flow in a porous medium).

Quasi steady state provides us with time-integrated or "mean" values for the water table, surface, and weathering front geometries. An interesting development would be to consider enriching our equations to compute the variability of these quantities. For example, the range of variability of the height of the water table would give us an estimate of the thickness of the region that experiences fluctuations in "wetness" and the distribution of timescales over which this happens.

The second type of approximations is geometrical. We have assumed uniform (and static) hydraulic, erosional, and chemical properties. As already mentioned in the description of the chemical model, we could easily improve it by introducing a cap on weathering rate (at high flow velocity) to incorporate the effect of dissolution reaction kinetics.

The hydraulic model assumes that the hydraulic conductivity is uniform and constant. The parameter K therefore represents the mean conductivity of the regolith layer. As mentioned earlier, we justify this approach by the observation that chemical weathering is often observed to take place across a rather thin front that separates unweathered bedrock from the overlying chemically altered regolith: the front commonly corresponds to a sharp transition in hydraulic properties that is therefore likely to be more important than any intraregolith variability. It is well known, however, that hydraulic properties (conductivity, permeability, and porosity) change with the evolution of the weathering profile [*White et al.*, 2001] and, to first order, with its thickening. A first-order improvement of the model would be to introduce a time- or depth-dependent hydraulic conductivity within the regolith layer. This is likely to have a noticeable impact if the variations in

hydraulic properties within the regolith are comparable in magnitude to the large jump in hydraulic properties across the weathering front.

It is well known that the precipitation of secondary minerals may lead to the formation of mechanically hard, resistant layers (ferricretes, calcretes, cangas, etc.) within the regolith profile. When these layers are later exhumed, they may alter the efficiency of surface erosion. This points to a potentially nonnegligible feedback between the weathering process and surface erosion which we have neglected here. There is evidence that the exhumation of hard layers or the hardening of the surface layer exerts what can sometimes appear as a dominant control on the shape of the landscape, but one must be careful in giving too much emphasis on what could be a rather transient phenomenon that contributes little to the long-term evolution of continental interiors. For example, ferricretes are commonly found at the top of hills, but it is not clear whether they "protect" the hill tops or whether they are more likely to be preserved there, because, by definition, hill tops are less eroded than valley bottoms. It is also important to note that the presence of a hardened layer or even the formation of soil may alter the hydrological properties of the system (hydraulic conductivity), which is not included in the present model.

6.3. Model Predictions and Behavior

6.3.1. Geometry of the Regolith

The main outcome of this work is that the distribution of regolith thickness is determined by the value of a single dimensionless number

$$\Gamma = \frac{KS^2}{P_0} \tag{80}$$

where S is surface slope, K regolith mean hydraulic conductivity, and P_0 infiltration rate which we take to be mostly controlled by precipitation rate (and thus climate). The value of this dimensionless number controls a first-order behavior of the system: whether the regolith layer is thicker near the top of topographic features or near their base (which we assume here is a local or regional base level for the aquifer bounded porous flow). This is true for both anorogenic and orogenic environments. In the later case, the mean slope of the surface of the hill, $\bar{S}$, must be used in the definition of the dimensionless number Γ.

In anorogenic settings, the distribution of regolith (and its connexion to surface slope) is set during the transition from fully saturated to fully unsaturated conditions. Considering the simple relationship we derived earlier (equation (24)) between the rate of regolith growth ($\partial B/\partial t$) and the rate of "desaturation" ($\partial x_s/\partial t$), we see that the constant of proportionality between the two (KS/P_0) is the ratio of the fluid velocity, KS, under saturated conditions to the precipitation rate, P_0 (or, more exactly, surface infiltration rate). In other words, what determines the geometry of the regolith layer is, ultimately, the ability of the regolith layer to evacuate through its base level water infiltrated through its surface. That the slope appears as a square in the expression of the dimensionless number comes from the combination of two factors: (1) that the rate of desaturation is proportional to the water flux (regardless of the nature of the weathering process) which, in a saturated medium, is proportional to slope and (2) that the evacuation of the water out of the regolith is accommodated by lateral flow.

During this transition from saturated to unsaturated conditions, the system is very susceptible to variations in Γ (i.e., precipitation rate or slope) as illustrated in Figure 13a where we show the results of a model run with parameters identical to the model shown in Figure 4 but where the precipitation rate has been forced to change abruptly 66.6 kyr into its evolution from 1 to 0.1 m/yr and later, at 133.1 kyr, back to its initial value of 1 mm/yr. We see that because the system has not fully reached its unsaturated state by the time the precipitation rate decreases, it changes its course from evolving toward producing a thicker regolith beneath the bottom of the hill ($\Gamma < 4$) toward producing a thicker regolith layer beneath the top of the hill ($\Gamma > 4$). The second change in precipitation rate forces the system to resume its evolution toward its initial target. The period of reduced precipitation rate causes, however, a perturbation in the regolith profile that is preserved in the final stage of evolution shown in Figure 13a as a marked change in basal slope (and regolith thickness). Once the system has become fully unsaturated, the geometry of the regolith layer becomes unaffected by variations in Γ (precipitation rate or slope), as the water table geometry is fully disconnected from the surface topography.

In orogenic settings, our model displays a more dynamical behavior as it always remains connected to the surface topography through the uplift/erosion process. Contrary to the predictions for anorogenic environments,

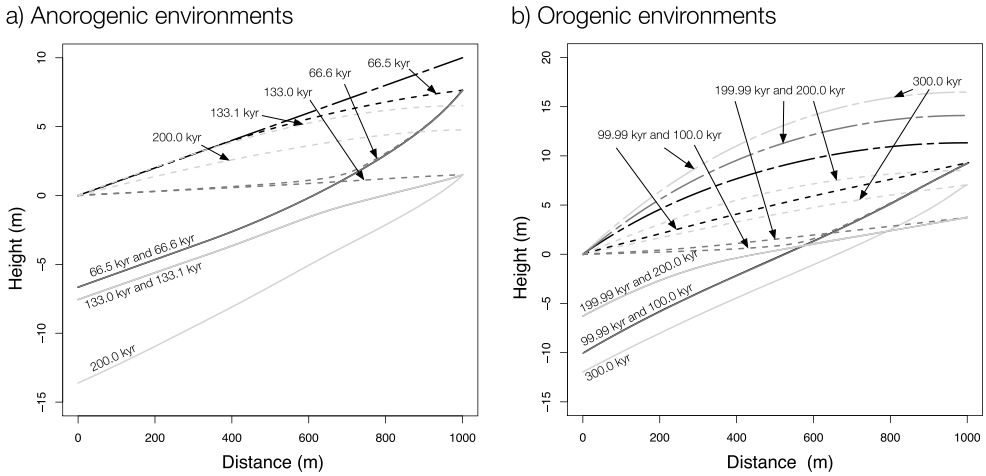


Figure 13. Time evolution of two model runs in which the precipitation has been arbitrarily decreased by a factor 10 between (a) 66.6 and 131 kyr and (b) 100 and 200 kyr. The solid lines represent the base of the regolith layer (or weathering front); the dashed lines represent the surface of the water table, and the dash-dotted lines represent the surface topography. (Figure 13a) No uplift, no erosion and constant slope. (Figure 13b) Imposed uplift and erosion causing a time-evolving surface topography.

the system tends toward a steady state geometry determined by the values of two dimensionless numbers, $\Gamma = K\bar{S}^2/P_0$ and $\Omega = FKL/2K_D$ (or $\Omega = FKS/\dot{\epsilon}$ under an arbitrary steady state surface). Changes in precipitation rate, for example, will change the value of Γ but not Ω and can, potentially, cause a substantial change in the geometry of the regolith. This is what is shown in Figure 13b where we have perturbed a model run identical to that shown in Figure 8a by decreasing the precipitation rate by a factor of 10, 100 kyr into its evolution, and later returning the precipitation rate to its initial value of 1 m/yr, 200 kyr into its evolution. The results show a marked change in regolith geometry from thickest beneath the base of the hill to thickest beneath the top of the hill between 100 and 200 kyr followed by a return to being thickest beneath the base. Contrary to the anorogenic system, these changes in regolith geometry result from absolute increase and decrease in regolith thickness at both the top and bottom of the hill: the regolith thickness decreases between 100 and 200 kyr at the base of the hill, whereas at the top of the hill it increases during the same period of time and decreases between 200 and 300 kyr.

That Γ is a strong function of surface slope, and a weaker function of precipitation and hydraulic properties (conductivity) implies that the distribution of regolith thickness as a function of surface slope could be used to validate this model and also to transform the model predictions into a simple algorithm to predict regolith thickness where it is not well constrained by direct measurements. Interestingly, our model makes a simple prediction about regolith thickness distribution that is independent of the rate at which weathering takes place. In other words, Γ is independent of F, the weathering rate coefficient. Unfortunately, Γ is a function of a poorly constrained quantity, K, the hydraulic conductivity.

Caution must, however, be used in interpreting these results as thick regolith profiles observed in anorogenic areas may have formed tens of millions of years ago, as shown by *Shuster et al.* [2012] by dating Mn oxides in regolith profiles from southeastern Brazil. For these ancient or relict profiles, it is difficult to be certain that present-day topography and slope are representative of the situation that prevailed when the profile formed.

We have also demonstrated that the value of the second dimensionless number, $\Omega = FKL/2K_D$ (or $\Omega = FKS/\dot{\epsilon}$ under an arbitrary surface geometry), controls the existence and mean thickness of the regolith profile. For regolith to be present at the base of the hill requires that $\Omega > 1/2$; for regolith to form at the top of the hill requires that $\Omega > 1$. We have also shown that, at steady state, the value of Ω can be directly measured from the ratio of the thickness of the regolith layer at the top of the hill to the height of the hill.

The value of Ω also affects the condition for regolith thickness distribution. We have shown that, in tectonically active environments, the condition for thicker soil at the base of the hill is

$$\Gamma < \Omega^2/(\Omega - 1) \tag{81}$$

This implies that the nearer the system is to the limit $\Omega \rightarrow 1$, the more likely the conditions for thicker soil near the base of the hill will be encountered, even for high slopes and/or low precipitation rates. When the system is far from that limit, i.e., $\Omega >> 1$, the conditions for thicker soil near the base of the hill are met when

$$\Gamma < \Omega \tag{82}$$

Contrary to Γ, Ω is a function of the weathering rate coefficient, F, which relates the fluid velocity to the weathering rate. In section 3.2, we tried to estimate its value from laboratory measurements and field observations. Interestingly, the steady state regolith thickness predicted by the model at the base of the hill (normalized by the total height of the hill) can be expressed as follows:

$$\frac{B_b^a}{z_t} = \frac{\Omega}{\Gamma} = \frac{FP_0}{\dot{\epsilon}\bar{S}} \tag{83}$$

which can be used to constrain the value of F from an independent estimate of surface erosion rate, assuming that the surface slope, the thickness of regolith near the base of the hill, and the mean precipitation (or net infiltration) rate are known/measurable, according to:

$$F = \frac{B_b^a}{z_t}\frac{\dot{\epsilon}\bar{S}}{P_0} \tag{84}$$

We show in section 6.4 how this can be done using an existing data set from India.

6.3.2. Time Evolution of the Regolith and Comparison to Previous Models

In anorogenic areas, i.e., under the assumption of a static surface geometry, no uplift and thus no erosion, our model does not tend toward steady state. We have also shown that, regardless of the geometry of the regolith layer, i.e., whether it is thickest near the top or near the bottom of the hill, the regolith thickness grows as the square root of time. This is a simple consequence of how fluid velocity (and thus weathering rate) decreases with increasing regolith thickness. We must, however, interpret this result with care, as our model is based on uniform and constant properties within the regolith layer and, most importantly, the hydraulic conductivity. It is clear, however, that, over time, the precipitation of secondary minerals and/or the formation of clays will lead to a potential local decrease in conductivity which will affect the rate of flow and thus the rate of weathering. This feedback could lead to the existence of a steady state solution.

It is interesting to note that *Lebedeva et al.* [2010] predict a similar behavior (regolith thickness increases as the square root of time) but based on an entirely different set of assumptions. In their model, the $\sqrt{t}$ evolution of regolith thickness is a consequence of the assumed competition between advective and diffusive solute transport which depends on the assumed fluid velocity.

Our model also predicts that, as the system evolves from a regolith free initial condition, it goes through a transitional phase where the regolith evolves from fully saturated conditions (the top of the water table is the surface of the hill) to fully unsaturated conditions (the top of the water table is fully decoupled from the surface of the hill). We have derived an analytical expression for the timescale of this transition. Interestingly, we found that it is independent of the assumed precipitation rate. This is because the precipitation rate controls both the geometry of the water table and also the geometry of the aquifer. The higher the precipitation rate, the steeper the water table but the faster the rate of weathering front propagation and thus regolith growth. During this transition period, the mean rate of regolith formation (total regolith thickness divided by the transition timescale) is equal to FKS and is independent of precipitation rate. For a given lithology (which should be the main control on F and K), the rate of regolith formation is thus directly proportional to slope.

In orogenic areas, our model implies that the regolith thickness will achieve a steady state value. This value and the geometry of the steady state regolith profile depend first on the value of the dimensionless parameter

$$\Omega = \frac{FKL}{2K_D} \tag{85}$$

or for an arbitrary surface topography

$$\Omega = \frac{FK\bar{S}}{\dot{\epsilon}} \tag{86}$$

As stated earlier, Ω is very similar to the second or erosional Damköhler number, which is defined as the ratio of the erosional timescale to the weathering timescale. The presence of a complete regolith profile on a given topographic feature implies that $\Omega > 1$, which in turn implies that the erosional response time of the system must be longer than its weathering response time. This implies that if the system has reached topographic (or erosional) steady state, it must have reached weathering steady state. In other words, where we think it is appropriate to assume that topographic steady state has been reached, the regolith profile (if it exists) is de facto at steady state. We can even take this reasoning one step further and assume that the distribution and thickness of regolith in an actively uplifting and eroding environment is, in general, likely to be at or near steady state. An alternate way of interpreting the meaning of Ω is to state that for values of $\Omega < 1$, a geomorphic system is production (in this case weathering) limited, whereas a system where $\Omega > 1$ is transport limited.

We have also shown that the value of the dimensionless parameters Ω and Γ can be extracted from simple measurements made about the regolith thickness, under the assumption that steady state has been reached (equations (75) and (76)). It is interesting to note too that our model predicts that Ω is also the ratio between the surface slope and the steady state slope of the water table (equation (48)). This implies that Ω is similar to the inverse of the dimensionless number derived by *Rempe and Dietrich* [2014a] in their "bottom-up" model yet under a very different set of assumptions that (i) the water table geometry is set by the hydraulic conductivity of an assumed permeable bedrock layer, that (ii) flow in the bedrock is arbitrarily confined to a depth corresponding the base of the hill, and that (iii) the weathering front (z_b, the limit between weathered and fresh, yet permeable, bedrock) is the surface of the water table. In our "top-down" approach, we do not impose that the weathering front is the surface of the water table. We note, however, that in situations characterized by high erosion rate ($\Omega \approx 1$) and/or steep topography ($\Gamma >> 1$), the ratio between the weathering front slope and the water table slope predicted by our model tends toward 1, as follows:

$$S_B/S_H = \frac{\partial(z - B^a)}{\partial x} \Big/ \frac{\partial H^a}{\partial x} = \bar{S}\left(\frac{\Omega}{\Gamma} + \frac{1}{\Omega}\right) \Big/ \frac{\bar{S}}{\Omega} = 1 + \frac{\Omega^2}{\Gamma} \rightarrow 1 \tag{87}$$

regardless of the surface topography slope. Consequently, the assumption of *Rempe and Dietrich* [2014a] that the water table is the weathering front becomes a prediction of our model in the peculiar circumstances of the site(s) they considered.

6.4. Comparison With Field Observations

In Figure 14, we illustrate the different regolith geometries predicted by the model through a set of observed profiles collected in the published literature from locations that are characterized by similar and close to world average precipitation rate (present-day rainfall in Eastern Senegal is 1200–1300 mm/yr, 911 mm/yr in the Southern Sierra, and 600–1200 mm/yr in the study area in Swaziland).

The first profile (Figure 14a) is from *Beauvais et al.* [1999]; it has been obtained by electric resistivity tomography of a thick lateritic mantle overlying granitic bedrock in southeastern Senegal. Most of the section is covered with a thick "glacis" not represented here. The environment is anorogenic, and surface slope is low (0.02). Assuming average values of $P_0 = 1$ m/yr and $K = 10^4$ m/yr leads to a value of $\Gamma = 4$ which, according to our model, is consistent with a regolith profile that is uniform in thickness from the hill top to its base level. This level would correspond, here, to the thalweg of nearby intermittently flowing rivers. This first example therefore corresponds to a situation where the surface slope is sufficiently low that the regolith layer thickens uniformly beneath topographic features. Note that this interpretation is only valid if the present-day topography (slope and position of topographic minima) is similar to the topography that overlaid the regolith profile during its formation.

The profile in Figure 14b is from an active tectonic or orogenic environment, i.e., the southern Sierra of California. The profile is from seismic refraction and electrical resistivity data collected by *Holbrook et al.* [2014] in a granitic landscape. The site and experimental setup are ideally suited to determine the geometry of the boundary between unweathered bedrock and the overlying regolith. The presence of regolith at the top of the hill indicates that uplift and erosion are not sufficiently rapid to prevent the formation of a regolith layer ($\Omega > 1$). Beneath the top of the hill, the regolith appears to extend to half the height of the hill, which we interpret to indicate that $\Omega \approx 2$, according to equation (47), and assuming erosional and weathering steady state. Surface slope is large (0.25), which implies a very large value for Γ and explains, according to our model, why regolith thickness is largest beneath the hill top ($\Gamma >> \Omega^2/(\Omega - 1)$).

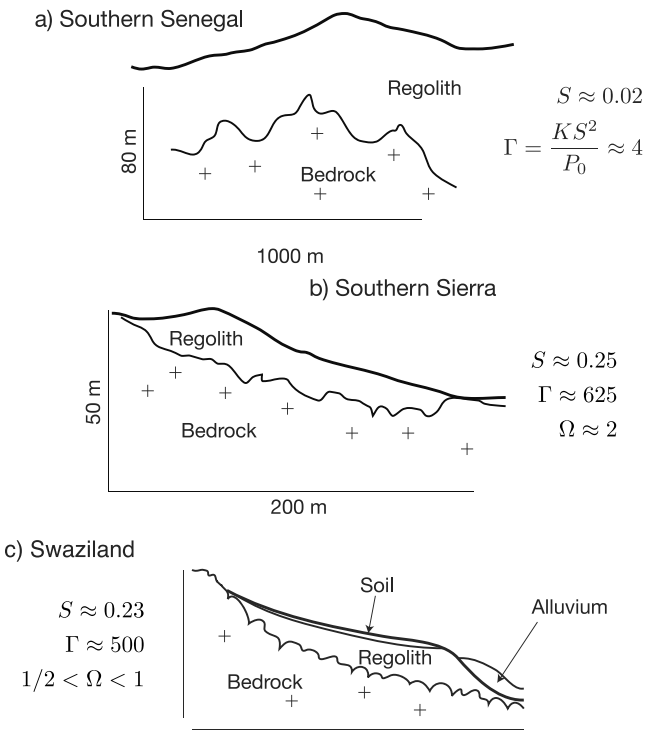


Figure 14. Regolith profiles obtained from (a, b) geophysical data and (c) field mapping. The thick line corresponds to the topographic surface and the thin line to the estimated base of the regolith (top of bedrock). Values of Γ are obtained by assuming a mean precipitation rate of 1 m/yr and a hydraulic conductivity of 10^4 m/yr. This choice is made to highlight the dominant effect of slope on the value of Γ. Ω is obtained from the ratio of regolith thickness to topographic height at the summit of the profile. The profiles are summarized versions of similar diagrams from (Figure 14a) *Beauvais et al.* [1999], (Figure 14b) *Holbrook et al.* [2014], and (Figure 14c) *Scholten and Henningsen* [1995].

The third profile (shown in Figure 14c) is a conceptual sketch of a "generalized toposequence" as observed in the middleveld region of central Swaziland by *Scholten and Henningsen* [1995] where mean hill slope is $\approx$ 0.23. The area is currently undergoing rapid erosion such that the tops of hills have been striped of their regolith layer to expose bare bedrock. According to our model, this implies that $\Omega < 1$ but because regolith is present at the base of the hill as well as intermediary elevations, it also implies that $\Omega > 1/2$. Note that this interpretation is based on the assumption that the erosional/weathering system has reached steady state, which may not be the case here. According to our model, the small value of Ω implies that the condition for a regolith layer thickening toward the topographic highs can never be reached despite the relatively large slope ($S = 0.23$).

6.5. How to Use This Model: Case Example of the Mule Hole Gneiss Watershed, South India

To demonstrate how our model (and its parameters) can be constrained by field measurements of regolith thickness and/or used to understand regolith formation at a specific site, we propose here to reanalyze the data set collected by *Braun et al.* [2009] in the Mule Hole watershed in India. We also show how our model can help put constraints on important timescales pertaining to weathering and regolith formation.

The Mule Hole watershed is located in the Kabini River basin in Karnataka State of southwestern India (see *Braun et al.* [2009] for exact location). It is approximately 4.3 km^2 in area (i.e., 3000×1500 m) and covered by a thick regolith. The protolith basement is made of the relatively heterogeneous Precambrian Peninsular Gneiss intermingled with a small amount (10–15%) of mafic and ultramafic volcano-sedimentary rocks. Regolith thickness is constrained by 12 electric resistivity tomography profiles [*Braun et al.*, 2009]. Although determining regolith thickness using contrast in electrical resistivity is tainted with relatively large uncertainties, estimates in the Mule Hole watershed range from 13.5 m at the outlet to 23.7 at the top, with a mean of $\approx$17 m [*Braun et al.*, 2009]. There is, however, no clear pattern between regolith thickness and elevation

or distance to the outlet [see *Braun et al.*, 2009, Figure 10]. The present-day catchment-averaged erosion rate determined by cosmogenic isotope analysis is $\dot{\epsilon} \approx 14 \times 10^{-6}$ m/yr [*Gunnell et al.*, 2007], and mean annual precipitation is approximately 1 m/yr.

From the regolith thickness information, we can derive the value of the two dimensionless numbers $\Omega = 2/(1 - B_t/z_t)$ and $\Gamma = 2\Omega(z_t/B_b)$, where z_t is the total elevation difference within the catchment (80 m) and B_t and B_b the regolith thickness at the top and bottom of the catchment. If we assume uniform regolith thickness, i.e., $B_t = B_b = 17$ m, we obtain $\Omega \approx 2.5$ and $\Gamma \approx 24$.

From these estimates, we can derive values for the model parameters, K and F, making basic assumptions about the better constrained parameters, S and P_0. The mean slope of the catchment is $S \approx 0.02$, and, being covered by a dry deciduous forest and affected by summer monsoons, infiltration rate should be a fraction only of mean annual rainfall, which we take to be $P_0 \approx 0.3$ m/yr. From this, we obtain that $K = \Gamma P_0/S^2 \approx 1.8 \times 10^4$ m/yr and $F = \Omega\dot{\epsilon}/KS \approx 10^{-7}$. The estimate for the hydraulic conductivity is within the expected range for regolith [*Bear*, 1979], but the value of the weathering rate coefficient, F, is rather low, i.e., an order of magnitude lower than what we had derived earlier from first principles (section 3.2). It is, however, consistent with the nature of the protolith, a hard metamorphic rock, which is very resistant to chemical weathering [*Meybeck*, 1987]. It also agrees with the conclusions of *Braun et al.* [2009] that the saprolitization process in the Mule Hole catchment is limited, based on measurements of major element loss from borehole samples.

From these estimates, we can derive that the weathering timescale (or time that was needed to achieve regolith thickness steady state) is $\tau = L/FK \approx 2.2$ Myr, the erosional timescale (or time that was needed to achieve erosional steady state) is $\tau_e = z_t/\dot{\epsilon} = \Omega\tau \approx 5.7$ Myr, and the hydrological timescale (or time it took for the regolith to evolve from saturated to unsaturated conditions) is $\tau_s = LP_0/FK^2S^2 = \tau/\Gamma \approx 90$ kyr. All of these timescales are important characteristic features of the system; they tell us, among other things, the time it would take for it to respond to changes in the forcing (tectonic uplift) or environment (climate, i.e., precipitation rate or rock type being exhumed). Weathering would take approximately 2 Myr to achieve a new steady state regolith thickness following a change in climate, while it would take approximately 5 Myr for topography to reach a new steady state geometry following a change in tectonic uplift rate. The short hydrological timescale says that, if perturbed in a way that parts of it became saturated, the system would rapidly adjust, by weathering, the geometry of the regolith to become fully unsaturated.

6.6. Need for a 2-D Model

There exist relatively extensive databases of regolith thickness measurements made in wells or boreholes [see, e.g., *Courtois et al.*, 2010]. To compare the predictions of our model to these observations requires to know or compute the base level to which the local water table connects. This level often corresponds to a river or a lake or, less frequently, to sea level. We are in the process of implementing a two-dimensional version of the weathering model we have presented here into a landscape evolution model that computes the geometry of the regional drainage network. We are coupling these two components such that the resurgence of water from the hydrological model is used to compute runoff and the emergence of a river network, which in turn is used to compute local hydrological base level. This is an obvious extension of the work presented here that should also allow to compute the regolith thickness and transport rate beneath hillslopes. We suspect that these strong couplings will lead to even more complex feedbacks between the various components of the system.

7. Conclusions

We have developed a new model for the formation of regolith by chemical weathering. The model combines existing concepts and ideas by coupling three basic partial differential equations controlling (1) the geometry of the water table within an aquifer of uniform properties which we associate to the regolith layer, (2) the geometry of the base of the regolith layer, and (3) the geometry of the surface topography, which is also the geometry of the top of the regolith layer. The novelty of our model is that it links the rate of propagation of the weathering front at the base of the regolith layer to the velocity of the fluid.

Under these assumptions, we are able to predict the geometry and rate of formation of the regolith. In anorogenic areas, our model predicts that the regolith layer thickness increases as the square root of time but never

Table 1. Summary of Timescales, Length Scales, Rates, and Dimensionless Numbers Derived From Our Analysis and Expressed in Terms of Model Parameters, Including Geometric Parameters L (Length of the Hill/Aquifer); S (Surface Slope); B_t and B_b (Regolith Thickness at the Top and Bottom of the Hill, Respectively); Environmental Parameters P_0 (Mean Infiltration Rate), U_0 (Uplift Rate), and $\dot{\epsilon}$ (Surface Erosion Rate); and Rock Properties F (Weathering Rate Coefficient), K (Hydraulic Conductivity), and K_D (Surface Transport Coefficient)

		Orogenic Systems	
	Anorogenic Systems	Hill Slope Diffusion	Arbitrary Surface
Desaturation timescale, τ_s	LP_0/FK^2S^2	$LP_0/4FK^2S^2$	$LP_0/4FK^2S^2$
Weathering timescale, τ	L/FK	L/FK	L/FK
Erosion timescale, τ_e	-	$L^2/2K_D = LS/U_0$	$LS/\dot{\epsilon}$
Regolith growth rate, $\partial B/\partial t$, during desaturation	FKS	$2FKS$	$2FKS$
Regolith growth rate, $\partial B/\partial t$, at steady state	-	$U_0 = 2K_DS/L$	$\dot{\epsilon}$
Desaturated regolith thickness, B_s	LP_0/KS	$LP_0/2KS$	$LP_0/2KS$
Steady state regolith thickness, B_t, at hill top	-	$LS - 2K_DS/FK$ $= LS - U_0L/FK$	$LS - \dot{\epsilon}L/FK$
Steady state regolith thickness, B_b, at hill bottom	-	FP_0L/U_0 $= FP_0L^2/2K_DS$	$FP_0L/\dot{\epsilon}$
Ω, controls regolith thickness	-	$FKL/2K_D = FKS/U_0$	$FKS/\dot{\epsilon}$
	-	$1/(1 - B_t/LS)$	$1/(1 - B_t/LS)$
Γ, controls regolith geometry	KS^2/P_0	KS^2/P_0	KS^2/P_0
	LS/B_s	$\Omega\, LS/B_b$	$\Omega\, LS/B_b$

reaches a steady state value. The geometry of the regolith is controlled by the value of a dimensionless number defined as follows:

$$\Gamma = \frac{KS^2}{P_0} \tag{88}$$

where K is the assumed hydraulic conductivity of the regolith, S is the surface slope, and P_0 the precipitation rate. For large values of Γ, which are most likely to be encountered for high surface slopes, regolith should be thickest near topographic highs. For small values of Γ, the model predicts that regolith should be thickest near topographic lows.

In orogenic areas, the presence of a regolith layer depends on the value of another dimensionless number which can be defined for a topographic feature of length L by

$$\Omega = \frac{KFL}{2K_D} \tag{89}$$

where F is the assumed dimensionless proportionality constant between flow rate and weathering front rate advance, i.e., the weathering rate constant, and K_D the assumed surface transport coefficient, relating slope to erosional/transport mass flux at the surface. Under an arbitrary surface topography, Ω can also be expressed as a function of the erosion rate, $\dot{\epsilon}$, and the mean steady state topographic slope, $\bar{S}$

$$\Omega = \frac{KF\bar{S}}{\dot{\epsilon}} \tag{90}$$

Our model predicts that for $1/2 < \Omega < 1$, regolith formation is limited to the lowest parts of the topography. To form regolith at the top of hills requires that $\Omega > 1$. Ω is also the ratio between the surface transport/erosional timescale and the weathering timescale, implying that where surface steady state has been reached and regolith is present on the landscape, weathering steady state must also be reached. Our model also predicts that the geometry of the regolith profile depends on the condition

$$\Gamma = \frac{KS^2}{P_0} \gtrless \frac{\Omega^2}{\Omega - 1} \tag{91}$$

This implies that, in general, soil will be thickest near the summit of topographic features in orogenic (or fast eroding) environments, unless Ω is small ($\Omega \leq 2$).

Because the values of Ω and Γ can be derived from simple point measurements of regolith thickness

$$\Omega = \frac{1}{1 - B_t/z_t} \quad \text{and} \quad \Gamma = \Omega\,(z_t/B_b) \tag{92}$$

where B_b and B_t are the regolith thicknesses at the bottom and top, respectively, of a hill of height z_t, our model is relatively easy to verify and/or used to interpret regolith profiles. We have demonstrated this by presenting a set of observed regolith profiles from three different environments for which we show that the first-order predictions of our model are likely to be correct. We have also used the model to extract estimates of model parameter values from field observations (surface slope, regolith thickness distribution, cosmogenic nuclide-derived rates of erosion, and precipitation rate) in a well-documented field site in India, as well as values for the various characteristic timescales, which inform us on the response times of the system to forcing or environmental changes.

In Table 1, we summarize the timescales, length scales, and rates that we have derived from our model under the assumptions of (1) no uplift/erosion (anorogenic systems), (2) uplift and slope-dependent surface transport (diffusive erosion), and (3) topographic and regolith steady state under an arbitrary surface topography. We also summarize the relationships between measurable steady state regolith thicknesses, B_t and B_b, and the dimensionless numbers, Γ and Ω.

Appendix A: Analytical Solution to Hydraulic Equation

If we assume that both topography, z, and regolith thickness, B, increase linearly with x

$$z = z_0 + Sx \quad \text{and} \quad B = B_0 + Sx \tag{A1}$$

and that both the permeability, K, and the precipitation rate, $P = P_0$, are constant, we obtain

$$K(H - z_0 + B_0)\,\frac{\partial H}{\partial x} = P_0(L - x) \tag{A2}$$

Introducing $H' = H - z_0 + B_0$, we can write

$$KH'\,\frac{\partial H'}{\partial x} = P_0(L - x) \tag{A3}$$

which has the following general solution:

$$H'(x) = \pm\sqrt{(P_0/K)\,x\,(2L - x) + c} \tag{A4}$$

and using the boundary condition $H'(0) = H_0 - z_0 + B_0$, we can determine c to obtain

$$H'(x) = \pm\sqrt{(P_0/K)\,x\,(2L - x) + (H_0 - z_0 + B_0)^2} \tag{A5}$$

and

$$H(x) = \sqrt{(P_0/K)\,x\,(2L - x) + (H_0 - z_0 + B_0)^2} + z_0 - B_0 \tag{A6}$$

neglecting the negative solution which does not have a physical sense. Note that in the special case where topographic variations are caused by regolith thickness variations, the solution is independent of the surface slope.

This solution is displayed (thin red line) in Figure A1 for $z_0 = 1$ m, $B_0 = 1$ m, $H_0 = 0.5$ m, $S = 0.01$, $L = 1000$ m, $P_0 = 1$ m/yr, and $K = 10^5$ m/yr.

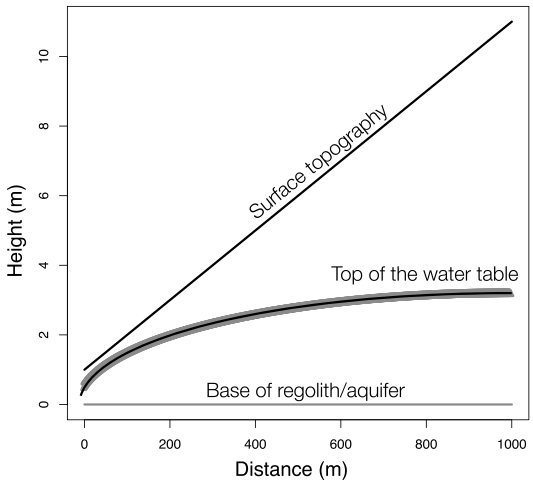


Figure A1. Comparison between analytical and numerical solutions corresponding to equation (A6). The thin black line represents the assumed topographic height; the grey line is the base of the regolith layer. The thick grey line is the computed surface of the water table using parameter values given in the text. The superposed black line is the analytical solution.

Appendix B: Hydraulic Equation Numerical Implementation

Equation (6) can be solved for arbitrary forms of both $z(x)$ and $B(x)$ using a simple first-order finite difference algorithm. Discretizing the problem to find the solution, H_i, at N equidistant points along a profile of length L gives

$$\frac{K}{2}(H_i - z_i + B_i + H_{i-1} - z_{i-1} + B_{i-1})\frac{H_i - H_{i-1}}{\Delta x} = F_i \tag{B1}$$

where F_i is the spatially integrated rainfall which can be easily computed from

$$F_{i-1} = F_i + P_{i-1}\Delta x \tag{B2}$$

where P_i is the precipitation rate at point i and $F_N = \Omega\Delta x/2$. Δx is the distance between two adjacent points, such that $(N-1)\Delta x = L$, and z_i and B_i are the topographic height and the regolith thickness at point i, respectively. In Figure A1 we compare the numerical solution (thick pink line) obtained for $N = 1001$ to the analytical solution given by equation (A6). For this problem where both surface elevation and regolith thickness vary linearly, the numerical solution is equal to the analytical solution within machine roundoff error, regardless of the discretization (value of N).

Appendix C: Fluid Velocity in the Fractured Bedrock

As shown in *Braun et al.* [2003], the focusing ratio, G^∞, or ratio of fluid steady state velocities in and outside of a thin layer characterized by an anomalous hydraulic conductivity, K_f, from the hydraulic conductivity, K, of the medium in which it is inserted is given by

$$G^\infty = \frac{v_f}{v} = \frac{\gamma}{1+\gamma}\delta \tag{C1}$$

where v_f and v are the fluid velocities in the anomalous conductivity layer and the surrounding medium, respectively.

$$\gamma = \frac{I}{W}\frac{K}{K_f} \tag{C2}$$

and

$$\delta = \frac{K_f}{K} \tag{C3}$$

where W and I are the thickness and vertical extent (length) of the anomalous conductivity layer.

In the case of the fractured bedrock layer at the base of the regolith $I = LS \approx 10$ m, $W \approx 10$ m, and $K/K_f \approx 10^2$ such that $\gamma \approx 10^2 >> 1$, and consequently,

$$G^{\infty} = \frac{v_f}{v} \approx \delta = \frac{K_f}{K} \tag{C4}$$

Acknowledgments
J. Mercier contributed to this work on a postdoctoral fellowship funded by Total SA. The authors wish to thank three anonymous reviewers for their very constructive comments which helped improve the manuscript. All data for this paper are properly cited and referred to in the reference list.

References

Ahnert, F. (1977), Some comments on the quantitative formulation of geomorphological processes in a theoretical model, *Earth Surf. Proc.*, *2*, 191–201.
Alexander, G. B., W. M. Heston, and R. K. Iler (1954), The solubility of amorphous silica in water, *J. Am. Chem.*, *58*(6), 453–455.
Anderson, S. P., and W. E. Dietrich (2002), Weathering profiles, mass-balance analysis, and rates of solute loss: Linkages between weathering and erosion in a small, steep catchment, *Geol. Soc. Am. Bull.*, *114*, 1143–1158.
Bear, J. (1979), *Hydraulics of Groundwater*, McGraw-Hill, New York.
Beauvais, A., M. Ritz, J. C. Parisot, and M. Dukhan (1999), Analysis of poorly stratified lateritic terrains overlying a granitic bedrock in West Africa, using 2-D electrical resistivity tomography, *Earth Planet. Sci. Lett.*, *173*, 413–424.
Berner, R. A. (1978), Rate control of mineral dissolution under Earth surface conditions, *Am. J. Sci.*, *278*, 1235–1252.
Berry, L., and B. P. Ruxton (1959), Notes on weathering zones and soils on granitic rocks in two tropical regions, *J. Soil Sci.*, *10*, 54–63.
Brantley, S. L., and A. F. White (2009), Approaches to modeling weathered regolith, *70*, 435–484
Braun, J., A. Heimsath, and J. Chappell (2001), Sediment transport mechanisms on soil-mantled hillslopes, *Geology*, *29*, 683–686.
Braun, J., S. Munroe, and S. Cox (2003), Transient fluid flow in and around a fault, *Geofluids*, *3*, 81–87.
Braun, J.-J., et al. (2009), Regolith mass balance inferred from combined mineralogical, geochemical and geophysical studies: Mule Hole gneissic watershed, South India, *Geochim. Cosmochim. Acta*, *73*(4), 935–961.
Carmo, I. O., and P. Vasconcelos (2004), Geochronological evidence for pervasive Miocene weathering, Minas Gerais, Brazil, *Earth Surf. Process. Landforms*, *29*(11), 1303–1320.
Carretier, S., Y. Goddéris, T. Delannoy, and D. Rouby (2014), Mean bedrock-to-saprolite conversion and erosion rates during mountain growth and decline, *Geomorphology*, *209*(C), 39–52.
Carson, M., and M. Kirkby (1972), *Hillslope Form and Process*, 475 pp., Cambridge Univ. Press, Cambridge, U. K.
Courtois, N., P. Lachassagne, R. Wyns, R. Blanchin, F. D. Bougaïré, S. Somé, and A. Tapsoba (2010), Large-scale mapping of hard-rock aquifer properties applied to Burkina Faso, *Ground Water*, *48*(2), 269–283.
Dupré, B., C. Dessert, P. Oliva, Y. Goddéris, J. Viers, L. François, R. Millot, and J. Gaillardet (2003), Rivers, chemical weathering and Earth's climate, *C. R. Geosci.*, *335*(16), 1141–1160.
Ferrier, K. L., and J. W. Kirchner (2008), Effects of physical erosion on chemical denudation rates: A numerical modeling study of soil-mantled hillslopes, *Earth Planet. Sci. Lett.*, *272*(3-4), 591–599.
Francois, L. M., and Y. Goddéris (1998), Isotopic constraints on the Cenozoic evolution of the carbon cycle, *Chem. Geol.*, *145*, 177–212.
Franklin, S. P., A. Hajash, T. A. Dewers, and T. T. Tieh (1994), The role of carboxylic acids in albite and quartz dissolution: An experimental study under diagenetic conditions, *Geochim. Cosmochim. Acta*, *20*, 4259–4279.
Gabet, E. J., and S. M. Mudd (2009), A theoretical model coupling chemical weathering rates with denudation rates, *Geology*, *37*(2), 151–154.
Gaillardet, J., B. Dupre, P. Louvat, and C. J. Allegre (1999), Global silicate weathering and CO_2 consumption rates deduced from the chemistry of large rivers, *Chem. Geol.*, *159*(1), 3–30.
Gilbert, G. (1877), *Report on the Geology of the Henry Mountains*, U.S. Geographical and Geological Survey of the Rocky Mountain Region, Washington, D. C.
Gleeson, T., K. M. Befus, S. Jasechko, E. Luijendijk, and M. B. Cardenas (2015), The global volume and distribution of modern groundwater, *Nat. Geosci.*, *9*(2), 161–167.
Goddéris, Y., and L. M. Francois (1995), The Cenozoic evolution of the strontium and carbon cycles: Relative importance of continental erosion and mantle exchanges, *Chem. Geol.*, *126*, 169–190.
Gunnell, Y., R. Braucher, D. Bourlès, and G. Andre (2007), Quantitative and qualitative insights into bedrock landform erosion on the South Indian craton using cosmogenic nuclides and apatite fission tracks, *Geol. Soc. Am. Bull.*, *119*(5-6), 576–585.
Heimsath, A., W. Dietrich, K. Nishiizumi, and R. Finkel (1997), The soil production function and landscape equilibrium, *Nature*, *388*, 358–361.
Heimsath, A., R. DiBiase, and K. Whipple (2012), Soil-production limits and the transition to bedrock-dominated landscapes, *Nat. Geosci.*, *5*, 210–214.
Herman, F., and J. Braun (2006), A parametric study of soil transport mechanisms, in *Tectonics, Climate, and Landscape Evolution*, vol. 398, edited by S. Willett et al., *Geol. Soc. of Am. Spec. Pap., 398*, Penrose Conference Series, pp. 191–200, doi:10.1130/2006.2398(11).
Hilley, G. E., C. P. Chamberlain, S. Moon, S. Porder, and S. D. Willett (2010), Competition between erosion and reaction kinetics in controlling silicate-weathering rates, *Earth Planet. Sci. Lett.*, *293*(1-2), 191–199.
Holbrook, W. S., C. S. Riebe, M. Elwaseif, J. L Hayes, K. Basler-Reeder, D. L Harry, A. Malazian, A. Dosseto, P. C Hartsough, and J. W Hopmans (2014), Geophysical constraints on deep weathering and water storage potential in the Southern Sierra Critical Zone Observatory, *Earth Surf. Process. Landforms*, *39*(3), 366–380.
Kooi, H. (2016), Groundwater flow as a cooling agent of the continental lithosphere, *Nat. Geosci.*, *9*(3), 227–230.
Lachassagne, P., R. Wyns, and B. Dewandel (2011), The fracture permeability of Hard Rock Aquifers is due neither to tectonics, nor to unloading, but to weathering processes, *Terra Nova*, *23*(3), 145–161.
Langston, A. L., G. E. Tucker, R. S. Anderson, and S. P. Anderson (2011), Exploring links between vadose zone hydrology and chemical weathering in the Boulder Creek critical zone observatory, *Appl. Geochem.*, *26*(S), S70–S71.
Lasaga, A. C., J. M. Soler, J. Ganor, and T. E. Burch (1994), Chemical weathering rate laws and global geochemical cycles, *Geochim. Cosmochim. Acta*, *58*, 2361–2386.
Lebedeva, M. I., and S. L. Brantley (2013), Exploring geochemical controls on weathering and erosion of convex hillslopes: Beyond the empirical regolith production function, *Earth Surf. Process. Landforms*, *38*(15), 1793–1807.
Lebedeva, M. I., R. C. Fletcher, V. N. Balashov, and S. L. Brantley (2007), A reactive diffusion model describing transformation of bedrock to saprolite, *Chem. Geol.*, *244*(3-4), 624–645.
Lebedeva, M. I., R. C. Fletcher, and S. L. Brantley (2010), A mathematical model for steady-state regolith production at constant erosion rate, *Earth Surf. Process. Landforms*, *35*, 508–524.

Lee, C. T. A., D. M. Morton, and M. G. Little (2008), Regulating continent growth and composition by chemical weathering, *Proc. Natl. Acad. Sci.*, *105*, 4981–4986.
Li, D. D., A. D. Jacobson, and D. J. McInerney (2014), A reactive-transport model for examining tectonic and climatic controls on chemical weathering and atmospheric CO_2 consumption in granitic regolith, *Chem. Geol.*, *365*(C), 30–42.
Lichtner, P. C. (1988), The quasi-stationary state approximation to coupled mass transport and fluid-rock interaction in a porous medium, *Geochim. Cosmochim. Acta*, *52*, 143–165.
Maher, K. (2010), The dependence of chemical weathering rates on fluid residence time, *Earth Planet. Sci. Lett.*, *294*(1–2), 101–110.
Maher, K. (2011), The role of fluid residence time and topographic scales in determining chemical fluxes from landscapes, *Earth Planet. Sci. Lett.*, *312*(1–2), 48–58.
Maher, K., and J. Druhan (2014), Relationships between the transit time of water and the fluxes of weathered elements through the critical zone, *Procedia Earth Planet. Sci.*, *10*, 16–22.
Martin, Y. (2000), Modelling hillslope evolution: Linear and nonlinear transport relations, *Geomorphology*, *34*, 1–21.
Martin, Y., and M. Church (1997), Diffusion in landscape development models: On the nature of basic transport relations, *Earth Surf. Process. Landforms*, *22*, 273–279.
Mayer, K. U., E. O. Frind, and D. W. Blowes (2002), Multicomponent reactive transport modeling in variably saturated porous media using a generalized formulation for kinetically controlled reactions, *Water Resour. Res.*, *38*(9), 1174–1195, doi:10.1029/2001WR000862.
Meybeck, M. (1987), Global chemical weathering of surficial rocks estimated from river dissolved loads, *Am. J. Sci.*, *287*, 401–428.
Moore, J., P. C. Lichtner, A. F. White, and S. L. Brantley (2012), Using a reactive transport model to elucidate differences between laboratory and field dissolution rates in regolith, *Geochim. Cosmochim. Acta*, *93*(C), 235–261.
Ortoleva, P., J. Chadam, E. Merino, and A. Sen (1987), Geochemical self-organization. II: The reactive infiltration instability, *Am. J. Sci.*, *287*, 1008–1040.
Pelletier, J. D., P. D. Broxton, P. Hazenberg, X. Zeng, P. A. Troch, G.-Y. Niu, Z. Williams, M. A. Brunke, and D. Gochis (2016), A gridded global data set of soil, intact regolith, and sedimentary deposit thicknesses for regional and global land surface modeling, *J. Adv. Model. Earth Syst.*, *8*, 41–65.
Phillips, J. D. (2005), Weathering instability and landscape evolution, *Geomorphology*, *67*(1–2), 255–272.
Rempe, D., and W. Dietrich (2014a), A bottom up approach to determining fresh bedrock topography under landscapes, *Proc. Natl. Acad. Sci.*, *111*(18), 6576–6581.
Rempe, D. M., and W. E. Dietrich (2014b), A bottom-up control on fresh-bedrock topography under landscapes, *Proc. Natl. Acad. Sci.*, *111*(18), 6576–6581.
Riebe, C. S., J. W. Kirchner, D. E. Granger, and R. C. Finkel (2001), Strong tectonic and weak climatic control of long-term chemical weathering rates, *Geology*, *29*, 511–514.
Riebe, C. S., J. W. Kirchner, and R. C. Finkel (2004), Erosional and climatic effects on long-term chemical weathering rates in granitic landscapes spanning diverse climate regimes, *Earth Planet. Sci. Lett.*, *224*(3–4), 547–562.
Rimstidt, J. D. (1997), Quartz solubility at low temperatures, *Geochim. Cosmochim. Acta*, *13*, 2553–2558.
Salve, R., D. M. Rempe, and W. E. Dietrich (2012), Rain, rock moisture dynamics, and the rapid response of perched groundwater in weathered, fractured argillite underlying a steep hillslope, *Water Resour. Res.*, *48*, W11528, doi:10.1029/2012WR012583.
Scholten, T., and P. F. Henningsen (1995), Morphogenesis and erodibility of soil-saprolite complexes from magmatic rocks in Swaziland (Southern Africa), *Z. Pflanzernernahr. Bodenk.*, *158*, 169–176.
Selby, M. (1993), *Hillslope Materials and Processes*, 451 pp., Oxford Univ. Press, Oxford, U. K.
Shuster, D. L., K. A. Farley, P. M. Vasconcelos, G. Balco, H. S. Monteiro, K. Waltenberg, and J. O. Stone (2012), Cosmogenic 3He in hematite and goethite from Brazilian "canga" duricrust demonstrates the extreme stability of these surfaces, *Earth Planet. Sci. Lett.*, *329-330*, 1–10.
Thomas, M. F. (1966), Some geomorphological implications of deep weathering patterns in crystalline rocks in Nigeria, *Trans. Inst. Br. Geogr.*, *40*, 173–19.
Vanwalleghem, T., U. Stockmann, B. Minasny, and A. B. McBratney (2013), A quantitative model for integrating landscape evolution and soil formation, *J. Geophys. Res. Earth Surf.*, *118*, 331–347, doi:10.1029/2011JF002296.
Vasconcelos, P. M., G. H. Brimhall, and T. A. Becker (1994), ^{40}Ar-^{39}Ar analysis of supergene jarosite and alunite: Implications to the paleoweathering history of the western USA and West Africa, *Geochim. Cosmochim. Acta*, *58*, 401–420.
West, A., A. Galy, and M. Bickle (2005), Tectonic and climatic controls on silicate weathering, *Earth Planet. Sci. Lett.*, *235*(1–2), 211–228.
White, A. F., T. D. Bullen, M. S. Schulz, and A. E. Blum (2001), Differential rates of feldspar weathering in granitic regoliths, *Geochim. Cosmochim. Acta*, *65*, 847–869.
Wilkinson, B. H. (2015), Precipitation as meteoric sediment and scaling laws of bedrock incision: Assessing the Sadler effect, *J. Geol.*, *123*(2), 95–112.
Yoo, K., S. M. Mudd, J. Sanderman, R. Amundson, and A. Blum (2009), Spatial patterns and controls of soil chemical weathering rates along a transient hillslope, *Earth Planet. Sci. Lett.*, *288*(1-2), 184–193.